Article

Choroid plexus-derived miR-204 regulates the number of quiescent neural stem cells in the adult brain

Tjasa Lepko[1,2,3,†], Melanie Pusch[1,†], Tamara Müller[4], Dorothea Schulte[4] (iD), Janina Ehses[5],
Michael Kiebler[5] (iD), Julia Hasler[1], Hagen B Huttner[6], Roosmarijn E Vandenbroucke[7,8,9] (iD),
Charysse Vandendriessche[7,8,9], Miha Modic[10,11], Ana Martin-Villalba[12] (iD), Sheng Zhao[12],
Enric LLorens-Bobadilla[12], Anja Schneider[13,14], Andre Fischer[15], Christopher T Breunig[16,17],
Stefan H Stricker[16,17], Magdalena Götz[1,3,18,‡] (iD) & Jovica Ninkovic[1,3,5,18,‡,*] (iD)

Abstract

Regulation of adult neural stem cell (NSC) number is critical for lifelong neurogenesis. Here, we identified a post-transcriptional control mechanism, centered around the microRNA 204 (miR-204), to control the maintenance of quiescent (q)NSCs. miR-204 regulates a spectrum of transcripts involved in cell cycle regulation, neuronal migration, and differentiation in qNSCs. Importantly, inhibition of miR-204 function reduced the number of qNSCs in the subependymal zone (SEZ) by inducing pre-mature activation and differentiation of NSCs without changing their neurogenic potential. Strikingly, we identified the choroid plexus of the mouse lateral ventricle as the major source of miR-204 that is released into the cerebrospinal fluid to control number of NSCs within the SEZ. Taken together, our results describe a novel mechanism to maintain adult somatic stem cells by a niche-specific miRNA repressing activation and differentiation of stem cells.

Introduction

Adult neural stem cells (NSCs) reside in few specific and restricted neurogenic niches of the mammalian brain (Weinandy *et al*, 2011; Ming & Song, 2012; Bond *et al*, 2015; Cameron & Glover, 2015) and generate neurons lifelong in the otherwise gliogenic environment (Ninkovic & Gotz, 2013). NSCs in the subependymal zone (SEZ) are heterogeneous differing in their stage of activation from quiescent (qNSC) to activated NSCs (aNSC; Codega *et al*, 2014; Llorens-Bobadilla *et al*, 2015). Lifelong neurogenesis in the adult brain relies on a population of qNSCs set apart during development (Fuentealba *et al*, 2015; Furutachi *et al*, 2015; Falk *et al*, 2017). Upon activation

1   Institute of Stem Cell Research, Helmholtz Center Munich, Neuherberg, Germany
2   Graduate School of Systemic Neurosciences, Ludwig-Maximilians Universitaet, Planegg-Martinsried, Germany
3   Physiological Genomics, Biomedical Center, Medical Faculty, Ludwig-Maximilians Universitaet, Planegg-Martinsried, Germany
4   Institute of Neurology (Edinger Institute), University Hospital, Goethe University Frankfurt, Frankfurt, Germany
5   Department for Cell Biology and Anatomy, Biomedical Center, Ludwig-Maximilians Universitaet, Planegg-Martinsried, Germany
6   Department of Neurology, University Hospital Erlangen, Friedrich-Alexander-University Erlangen-Nürnberg, Erlangen, Germany
7   VIB Center for Inflammation Research, VIB, Ghent, Belgium
8   Department of Biomedical Molecular Biology, Ghent University, Ghent, Belgium
9   Ghent Gut Inflammation Group (GGIG), Ghent University, Ghent, Belgium
10 The Francis Crick Institute, London, UK
11 Department for Neuromuscular Diseases, UCL Queen Square Institute of Neurology, London, UK
12 Molecular Neurobiology, German Cancer Research Center (DKFZ), Heidelberg, Germany
13 Translational Dementia Research Group, German Center for Neurodegenerative Diseases (DZNE) Bonn, Bonn, Germany
14 Department of Neurodegenerative Diseases and Geriatric Psychiatry, University Clinic Bonn, Bonn, Germany
15 Department for Epigenetics and Systems Medicine, German Center for Neurodegenerative Diseases (DZNE) Göttingen, Göttingen, Germany
16 MCN Junior Research Group, Munich Center for Neurosciences, BioMedical Center, Ludwig-Maximilians Universitaet, Planegg-Martinsried, Germany
17 Epigenetic Engineering, Helmholtz Zentrum München, Neuherberg, Germany
18 Munich Cluster for Systems Neurology (SyNergy), Munich, Germany
    *Corresponding author. Tel: +49 89 2180 71633; E-mail: ninkovic@helmholtz-muenchen.de
    †These authors contributed equally to this work
    ‡These authors contributed equally to this work

within the adult brain, the vast majority of these once quiescent cells will produce only a few cohorts of neurons before being depleted (Bonaguidi *et al*, 2011; Calzolari *et al*, 2015) or return to quiescence (Basak *et al*, 2018). Therefore, an important cornerstone in understanding the regulation of neurogenesis within the adult brain, including its age-related decline (Shook *et al*, 2012), is to decipher mechanisms controlling the balance between qNSC maintenance and activation. The neurogenic niche harboring NSCs has been proposed to be the key to control this balance and maintain the neurogenic potential in specific, spatially restricted brain areas (Donnelly *et al*, 2018). These niches provide unique support for neurogenesis, as the brain parenchyma outside these niches limits the neurogenic potential of endogenous or transplanted neuronal progenitors (Flax *et al*, 1998; Winkler *et al*, 1998; Fricker *et al*, 1999; Englund *et al*, 2002). Individual proteins, such as extracellular matrix (ECM) proteins, *for example,* tenascin-c (Tnc) and thrombospondin 4 (Thbs4; Garcion *et al*, 2001; Girard *et al*, 2014), have already been described as integral part of the neurogenic niche in the adult murine brain. To date, various signaling factors have been reported to regulate adult neurogenesis, such as SHH (Ihrie *et al*, 2011), WNT (Azim *et al*, 2014), BMP (Lim *et al*, 2000; Colak *et al*, 2008), and ephrins (Conover *et al*, 2000; Nomura *et al*, 2010) with only few regulating the maintenance of qNSCs in the SEZ, such as PEDF (Ramirez-Castillejo *et al*, 2006) or components of the cerebrospinal fluid (Codega *et al*, 2014; Silva-Vargas *et al*, 2016; Petrik *et al*, 2018). Likewise, transcriptional networks and gene regulatory elements have been described to regulate fate progression from NSCs to neuroblasts (Lim *et al*, 2000, 2009; Brill *et al*, 2008; Mu *et al*, 2012; Ninkovic *et al*, 2013; Ramos *et al*, 2013, 2015; Luo *et al*, 2015; Dulken *et al*, 2017; Zywitza *et al*, 2018; Baser *et al*, 2019), but little is known about post-transcriptional control mechanisms maintaining NSC quiescence.

Here, we set out to identify novel regulators of NSC maintenance. Genome-wide expression analysis had shown that NSCs express low levels of mRNAs for neurogenic fate determinants and proliferation regulators that then further increase during lineage progression along with appearance of the respective proteins (Beckervordersandforth *et al*, 2010). We reasoned that post-transcriptional mechanisms defining transcript and/or protein levels of these fate determinants and cell cycle regulators would be excellent candidates to control the balance between NSC differentiation and long-term maintenance.

Results

qNSCs are primed toward neurogenesis

To identify factors controlling NSC activation and quiescence, we set out to compare the transcriptome of freshly isolated NSCs (hGFAP-GFP$^+$; CD133$^+$), and hGFAP-GFP$^+$ astrocytes without stem cell capacity from the diencephalic parenchyma (to avoid contamination with stem cells residing at the ventricular wall of 3rd ventricle; for more details, see Beckervordersandforth *et al*, 2010). Surprisingly, we observed the expression of neurogenic fate determinants already in the NSC (Beckervordersandforth *et al*, 2010 and Table EV1). The qPCR validation of these data showed that neurogenic fate determinants such as MEIS2 (Agoston *et al*, 2014; Hau *et al*, 2017), SOX11 (Mu *et al*, 2012), or PAX6 (Ninkovic *et al*, 2013) were already expressed in both activated, EGFR-positive NSCs

(aNSCs) and quiescent, EGFR-negative NSCs (qNSCs), but virtually absent in diencephalic astrocytes (Figs 1A and EV1A). The expression levels of these neurogenic fate determinants further increased in the prospectively isolated progeny of NSCs, such as neuroblasts (Figs 1A and EV1A, and Table EV1; see Beckervordersandforth *et al*, 2010; Codega *et al*, 2014; Fischer *et al*, 2011, for the sorting procedure). We then asked whether low expression of neurogenic fate determinants is a general feature of the NSC-specific transcriptome. As there are several approaches aiming at the identification of stem cell-specific transcriptome (Beckervordersandforth *et al*, 2010; Codega *et al*, 2014; Llorens-Bobadilla *et al*, 2015), we chose to overlay them to identify a common NSC signature (Fig EV1B). Common genes were then analyzed for their expression in parenchymal diencephalic astrocytes and SEZ neurogenic lineage. We identified 74 genes (Fig EV1B and Table EV2) with low or absent expression in astrocytes and increasing levels from NSC to neuroblasts. Some of these genes exhibited up to 100× higher mRNA levels in NSCs compared to bona-fide astrocytes isolated from the diencephalon (Table EV1). Collectively, these 74 genes are enriched for GO categories encompassing cell cycle, neuronal differentiation, and migration (Fig EV1C and Table EV3).

To examine how this transcriptional regulation is reflected at the protein level in qNSCs, we used immunohistochemistry (IHC) for two factors following the above described expression pattern: MCM6, a transcription factor regulating proliferation (Noseda & Karsan, 2006), and MEIS2, regulating neurogenesis in the SEZ (Agoston *et al*, 2014; Hau *et al*, 2017). We used a long-term BrdU label-retaining protocol (Codega *et al*, 2014) allowing detection of a subset NSCs and their progeny. Eight-week-old animals received BrdU in drinking water for 2 weeks followed by a 2-week chase period. During the chase period, fast dividing cells dilute the label below detectable level. Differentiating NSC progeny that keep the BrdU label and migrate to the RMS and OB as well as neuroblasts that still remain in the SEZ were excluded from the analysis using DCX immunostaining. Cells immunopositive for BrdU only are those that divided only few times during the labeling period and therefore represent a subset of qNSCs [from here onwards referred as label-retaining cells (LRCs)]. To identify the size of the LRC cohort, we dissociated the SEZ from hGFAP-eGFP$^+$ animals and observed that 24.0 ± 7.7% of NSCs (hGFAP-GFP$^+$ and CD133$^+$) were LRCs (Fig EV1D). Immunostaining in the SEZ *in vivo* revealed 63.4 ± 5.6% of qNSCs immunonegative for MEIS2 protein (Fig 1B, C and E) and 86.5 ± 3.3% for MCM6 (Fig 1D and E). We further asked whether MEIS2-negative LRCs express any *Meis2* RNA. Therefore, we combined flourescent ISH (FISH) detecting *Meis2* mRNA and immunostaining for MEIS2 protein on either SEZ tissue or acutely isolated SEZ cells. Both approaches identified LRCs expressing *Meis2* mRNA with low or undetectable MEIS2 protein (Fig 1B and Movie EV1). Moreover, the intensity of FISH signal increased from DCX-negative LRCs to neuroblasts (Fig 1B and Movie EV1) in line with our transcriptome analysis on sorted NSCs and their progeny. Taken together, a notable discrepancy exists between *Meis2* and *Mcm6* transcript expression and protein production of these neurogenic determinants in qNSCs. This raises the intriguing possibility that qNSCs are primed for neurogenesis as they already express the transcriptional program to implement proliferation and neuronal differentiation but are held back from acting on it by post-transcriptional mechanisms.
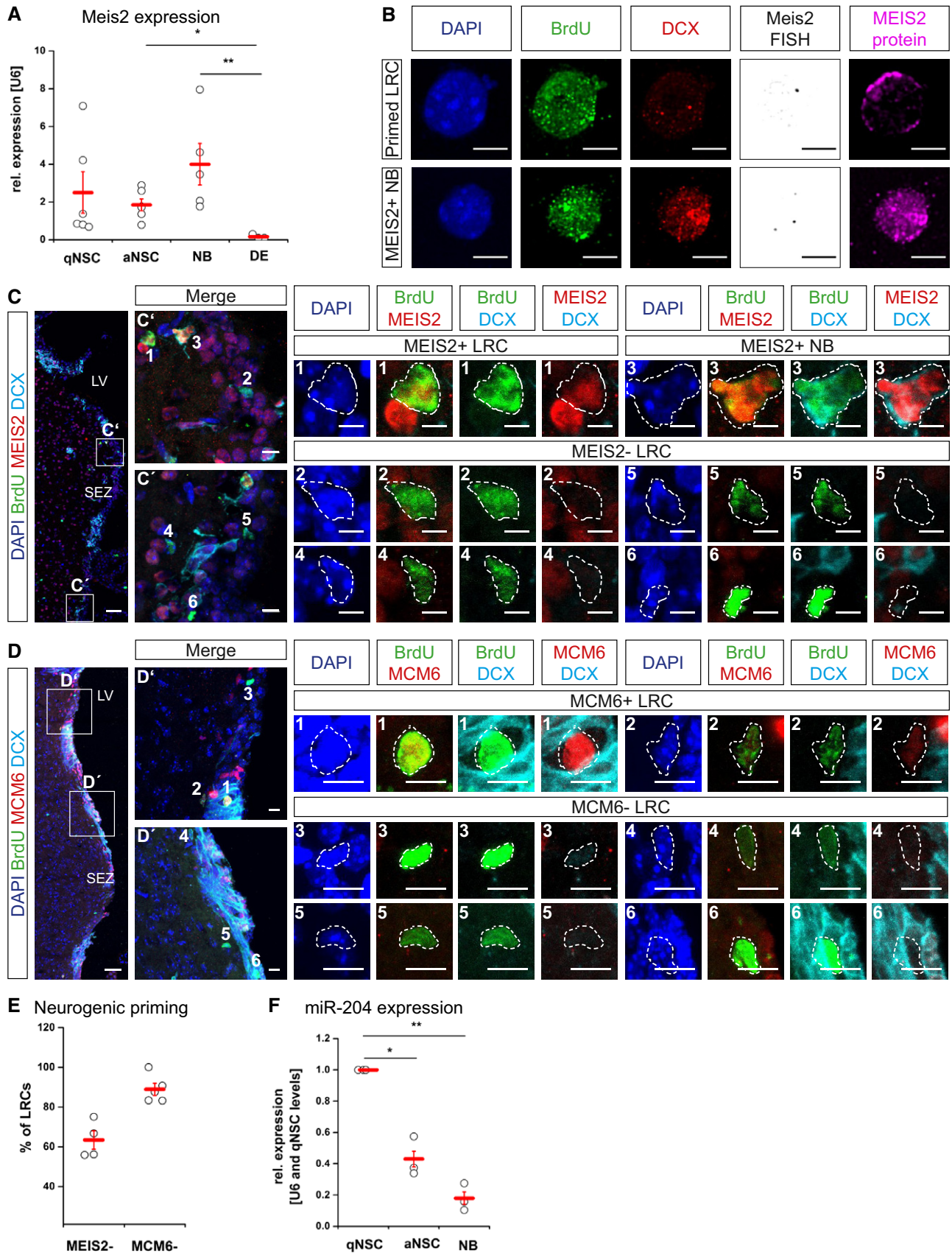
Figure 1.

Figure 1. A subset of qNSCs (LRCs) expresses mRNA but not the protein for neurogenic fate determinants.

A   Dot plot depicting the expression of mRNA for neurogenic transcription factor MEIS2 in prospectively isolated cellular populations from the SEZ.
B   Micrographs depicting the expression of neurogenic fate determinant *Meis2* mRNA and MEIS2 protein in acutely dissociated SEZ cells. Note that *Meis2* mRNA-positive LRCs have low (no) MEIS2 protein.
C, D   IHC labeling for MEIS2 (C) and MCM6 (D) of LRCs positive for BrdU-only and neuroblasts marked by DCX.
E   Dot plot showing the proportion of BrdU$^+$ LRCs negative for MEIS2 or MCM6 protein.
F   Dot plot depicting the expression of miR-204 in prospectively isolated cells of neural lineage.

Data information: See also Fig EV1. All fluorescent images are full *Z*-projections of confocal *Z*-stack. Boxed areas correspond to the higher magnification images in adjacent panels (C', C′, D', and D′); numbers (1–6) label the position of the cells zoomed in the adjacent panels (C', C′, D', and D′). Abbreviations: qNSC, quiescent neural stem cell; aNSC, activated neural stem cell; NB, neuroblast; DE, diencephalon astrocytes; LRC, label-retaining cell; SEZ, subependymal zone; LV, lateral ventricle. Data are shown as mean $\pm$ SEM; each single dot represents independent biological replicate; significance was tested by non-parametric Kruskal–Wallis ANOVA; *P value < 0.05, **P value < 0.01. Scale bars (C, D) 50 μm, (C', C′, D', D′), 10 μm (B, numbered magnifications) 5 μm.

miR-204 controls neurogenic priming of adult NSCs

The apparent discrepancy between mRNA expression but absent or very low protein load of several neurogenic fate determinants in most LRCs (Fig 1B, Movie EV1) prompted us to search for microRNAs (miRNAs) that may control levels of these proteins (common genes in Fig EV1B). Since the regulation through miRNAs largely depends on complementary base pairing of their seed sequence to the 3′-UTR of the target mRNA, we used a combination of online target prediction tools (TargetScan, MiRanda, starBase, and miRSearch (http://www.exiqon.com/microrna-target-prediction and references therein) to search 3′ UTRs of known neurogenic factors. We hypothesized that the relevant regulatory miRNA should target several neurogenic fate determinants. Indeed, we identified a number of miRNAs with putative binding to the 3′-UTR of multiple neurogenic fate determinants (Table EV1). miR-204 mapped to the 46% of these factors (Fig EV1E and F, and Table EV2), including known miR-204 targets *Sox11* and *Meis2* (Conte *et al*, 2010; Shaham *et al*, 2013). Moreover, it is one of the most abundant miRNAs in the brain (Wang *et al*, 2017), making it a prime candidate for regulating the potential of NSCs. Importantly, miR-204 regulated the firefly luciferase mRNA fused to the 3′-UTR of *Meis2*, *Mcm6*, *Arx*, *Dlx1*, *Dlx2,* and *Sox11* in luciferase reporter assays (Fig EV1G). A point mutation in the seed sequence for miR-204 within the 3′UTR of these neurogenic factors either entirely abolished or interfered with this regulation (with the exception of *Sox11*), supporting the direct miR-204-mediated regulation of selected neurogenic fate determinants. *Sox11* 3′UTR has several imperfect binding sites for miR-204 possibly accounting for the remaining regulation that we observed in the mutated 3′UTR. GO term analysis (DAVID) of the predicted miR-204 targets (Table EV2) showed enrichment of categories involved in neuronal differentiation and cell cycle control (Fig EV1H and Table EV4), overlapping with the GO terms of primed genes as shown above (Fig EV1C). Notably, the level of mature miR-204 was highest in freshly isolated qNSCs and lower in aNSCs and NBs (Fig 1F) further corroborating a possible role of miR-204 in the regulation of neurogenic priming.

To examine the role of miR-204 in neurogenic priming of qNSCs, we interfered with its function in the adult SEZ *in vivo* by injection of miR-204 specific antagomirs (AntimiR204) into the lateral ventricle (Wang *et al*, 2012). We first labeled a subset of qNSCs using the BrdU retaining protocol as described above and injected after the first week of the chase period miR-204 specific antagomirs (AntimiR) or artificial CSF control (vehicle used for antagomirs) into the lateral ventricle (Fig 2A). As the *in vivo* antagomirs carry

O-methylation, they enter cells in direct contact with the lateral ventricle, including NSCs, ependymal cells, and choroid plexus (ChP). Indeed, already 3 days after injection, the levels of miR-204 were reduced in the ChP and SEZ isolated from animals treated with the antagomirs compared to animals treated with CSF control (Fig EV2A and B). To evaluate the effect of miR-204 loss of function on neurogenic priming, we assessed the number of LRC with detectable protein levels for MEIS2 (Fig 2B–D) in miR-204-deficient and control animals. Indeed, we observed a significant increase in the proportion of LRCs immunopositive for MEIS2 protein after miR-204 inhibition compared to control animals (Fig 2B–D). These data, therefore, support a functional role of miR-204 in keeping qNSCs undifferentiated but primed for rapid neurogenesis.

Loss of neurogenic priming leads to pre-mature differentiation of qNSCs

To examine whether miR-204 mediated priming is important for the maintenance of qNSCs, we compared the number of BrdU label-retaining qNSCs, negative for Ki67 and for DCX, in miR-204-deficient and control animals (Fig 3A–C). Loss of miR-204 function reduced the number of label-retaining qNSCs to 53% of the number of LRCs observed in the animals injected with vehicle already 7 days after injection (Fig 3A–C). Moreover, we observed a trend toward reduced numbers of Ki67$^+$, DCX$^-$ aNSCs and transit amplifying progenitors (Fig 3A, B and D). The decrease in number of LRCs is likely not due to selective cell death as almost no TUNEL$^+$ cells could be detected in the SEZ in either condition at 7 days after injection (Fig EV2C and D). However, we cannot exclude cell death-mediated effects at earlier stage. In contrast, DCX-positive NBs increased 1.6-fold compared to controls in the SEZ of miR-204 antagomir-injected mice (Fig 3A, B and E) without an obvious effect on their proliferation (no change in proportion of Ki67$^+$ DCX$^+$ cells among all DCX$^+$ cells). We also observed a significantly increased number of BrdU$^+$ cells (progeny of NSCs) in both RMS and OB of animals treated with the miR-204-specific antagomirs compared to controls (Fig 3F–H). Considering that, by virtue of our labeling protocol, BrdU$^+$ cells must be progeny of LRCs, this observation indicates that BrdU$^+$ qNSCs may begin to differentiate when miR-204 is depleted. Notably, miR-204 inhibition did not change the fate of NSC progeny, as the proportion of newly generated neuroblasts among all BrdU labeled cells did not differ between the two conditions (Fig EV2E and F).

In order to understand the molecular mechanism underlying the decrease in number of LRCs in the SEZ, we compared the
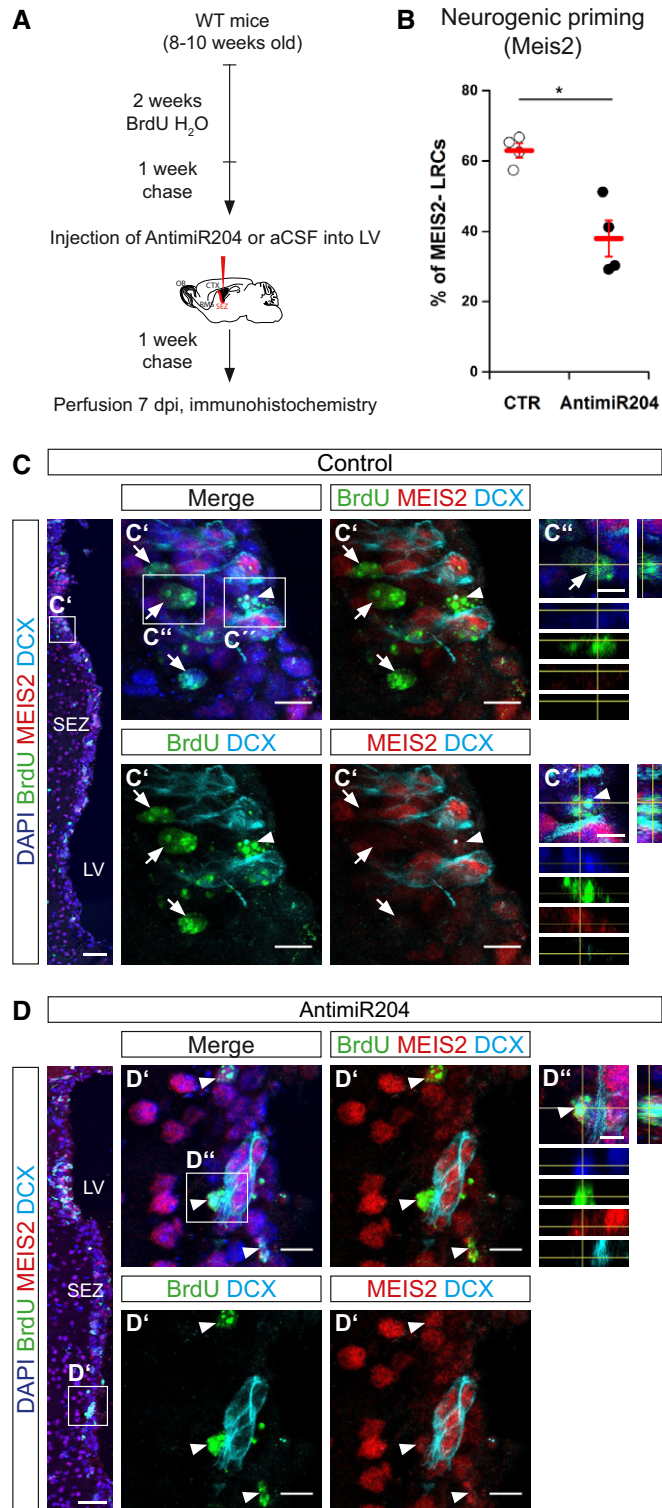
Figure 2. miR-204 regulates neurogenic priming of adult NSCs.

A Schematic representation of the experimental workflow for labeling LRCs with BrdU in the adult SEZ and miR-204 inhibition using antagomirs.

B Dot plot depicting the immunoreactivity of LRCs for MEIS for MEIS2 in control and antagomirs treated animals 7 dpi.

C, D Micrographs showing IHC for the neurogenic priming factor MEIS2 in the SEZ 7 days after injection of artificial CSF (control, C) or AntimiR204 (D). White arrows indicate LRCs without detectable MEIS2 protein. The white arrowheads are pointing out the loss of neurogenic priming (LRCs positive for MEIS2 protein) upon the antagomir treatments.

Data information: See also Fig EV1. All fluorescent images are full Z-projections of confocal Z-stack, orthogonal projections are single plane pictures. Boxed areas correspond to the higher magnification images in adjacent panels (C', D') or orthogonal projections (C'', C''', D''). Abbreviations: AntimiR, antagomir; aCSF, artificial cerebrospinal fluid; CTR, control; SEZ, subependymal zone; LV, lateral ventricle; WT, wild type; dpi, days post-injection; LRC, label-retaining cell; OB, olfactory bulb; CTX, cortex; RMS, rostral migratory stream. Data are shown as mean ± SEM; each symbol represents independent biological replicate; significance was tested by non-parametric Kruskal–Wallis ANOVA; *P value < 0.05. Scale bars (C, D) 50 μm, (C', D') 10 μm, (C'', C''', D'') 5 μm.

of priming factors that had been sensitive to miR-204 in the luciferase assay (Fig EV1G) exhibited elevated transcript levels in qNSCs following loss of miR-204 function compared to the levels in control animals (Fig EV3A and B). Moreover, the transcriptome comparison identified both up- and down-regulated genes (419 up-regulated and 357 down-regulated, twofold up-regulation, $P < 0.05$, Table EV5), suggesting that we observe a change in the transcriptomic signature of miR-204-deficient qNSCs rather than only increased level of direct miR-204 targets. The GO terms overrepresented in this gene set (twofold enrichment, $P < 0.05$ and at least five genes in the GO category) were linked to the cell cycle, neurogenesis, synaptogenesis, and neuronal migration (Fig EV3C and D, and Tables EV6 and EV7), all processes that are consistently enriched in the set of neurogenic priming genes (Fig EV1).

Taken together, reduced levels of miR-204 lead to activation and depletion of qNSC pool in the SEZ reflected by the reduction in number of LRCs and increased neuroblast production.

Choroid plexus releases miR-204

Given the important role of miR-204 in controlling the number of qNSCs, we aimed to determine the origin of miR-204. We first examined the expression of miR-204 throughout the adult brain by *in situ* hybridization and found high expression exclusively in the choroid plexus (ChP; Fig 4A, A' and A'' and Deo *et al*, 2006). The amount of miR-204 was 120-fold higher in the ChP compared to the SEZ tissue (Fig 4B). Given that NSCs are in direct contact with the cerebrospinal fluid (CSF), we hypothesized that the ChP could be the main source of miR-204, releasing it into the CSF. Consistent with this hypothesis, we detected miR-204 but not the small spliceosomal RNA U6 in the CSF, excluding cellular contamination (Fig 4C). Isolation of extracellular vesicles (EVs) from human CSF (Fig 4D and E) showed enrichment of mature miR-204 in the CSF fraction containing EVs when compared to the EVs free fraction (Fig 4E and F). To further verify that EVs contain miR-204, we blocked EV secretion from the ChP by addition of the neutral sphingomyelinase inhibitor GW4869, a validated inhibitor of EVs production (Trajkovic *et al*, 2008; Balusu *et al*, 2016). GW4869

transcriptome of prospectively isolated qNSCs (hGFAP-GFP⁺; CD133⁺; EGFR⁻) deficient for miR-204 with the qNSC isolated from control, sibling brains. This analysis was performed 3 days after a single ventricular injection of AntimiR204, a time point at which we did not observe any change in number of LRCs. Importantly, most
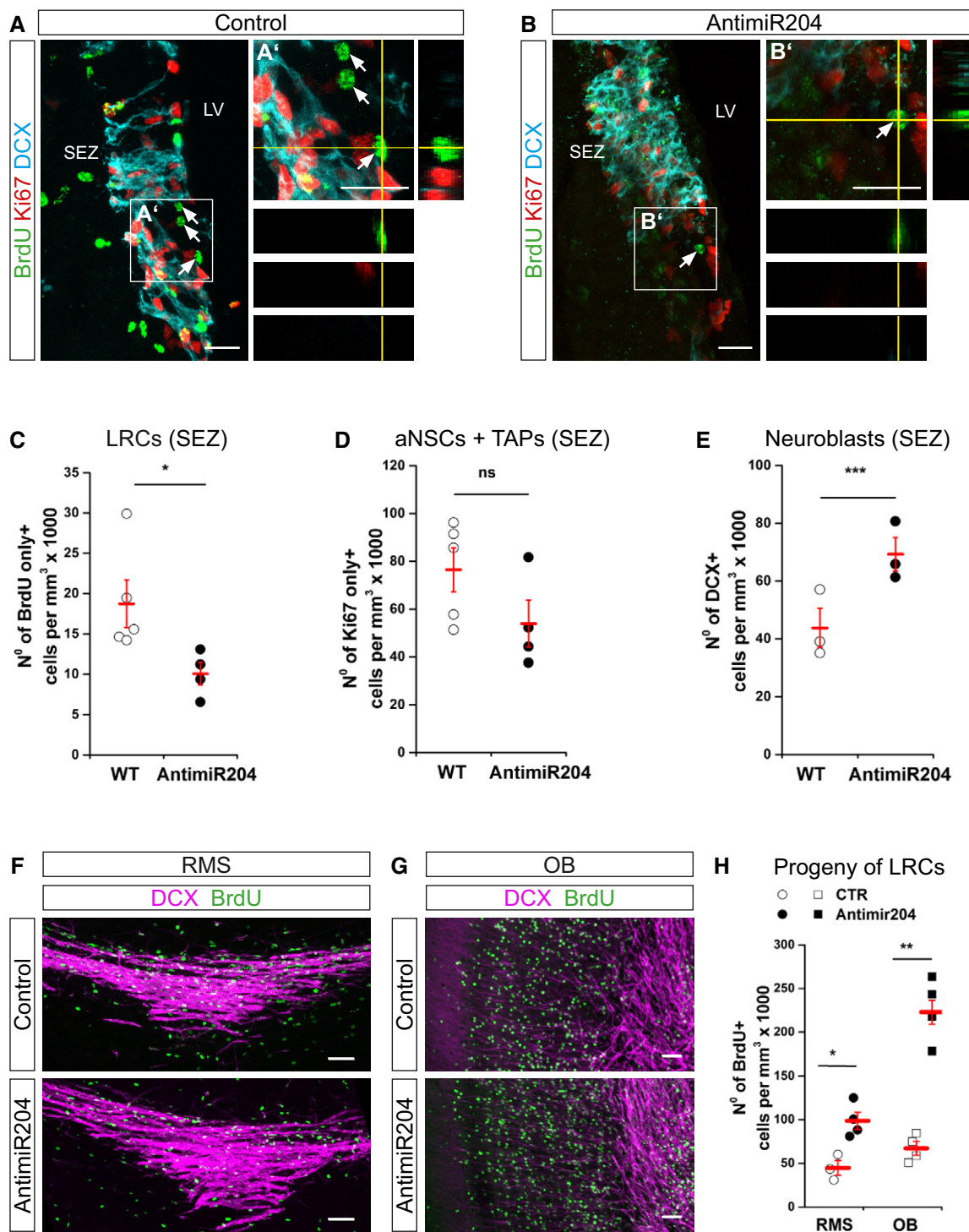
Figure 3.

inhibitor or vehicle was injected into the lateral ventricle, EVs were isolated from CSF after 2 h, imaged with transmission electron microscopy (Fig 4G), and analyzed for miR-204 levels by real-time (RT) qPCR. Inhibition of EV production significantly reduced the amount of miR-204 in the CSF (Fig 4H), further corroborating that miR-204 is predominantly released from the ChP into the CSF within EVs.

We next asked whether NSCs could take up miR-204 from the CSF. To address this question, we used primary SEZ cultures containing NSCs (Ortega *et al*, 2011) that do not express miR-204 (Figs 5A and EV4A). When these cells were analyzed in trans-well assays together with ChP explants allowing only exchange of EVs and secreted/released molecules (Fig EV4A), miR-204 was detectable both in the culture medium (Fig 5B) and in the primary SEZ

Figure 3.   Loss of the neurogenic priming *in vivo* induces pre-mature differentiation of adult NSCs.

A, B   Micrographs depicting the cellular composition in the SEZ 7 days after injection of aCSF (control, A) or AntimiR204 (B). Boxed areas correspond to higher magnifications in adjacent panels (A', B').

C–E   Dot plots depicting the abundance of LRCs (BrdU$^+$, Ki67$^-$, DCX$^-$), aNSCs and TAPs (BrdU$^-$, Ki67$^+$, DCX$^-$) and neuroblasts (DCX$^+$ Ki67$^+$ or DCX$^+$ Ki67$^-$) in the SEZ 7 days after aCSF or AntimiR204 injection. Note that the number of LRCs (white arrows in A and B) is reduced in Antimir204 injected SEZ, while the number of NBs is increased.

F, G   Micrographs depicting the elbow—the most ventral region of the RMS (F) and OB neuronal layers (G) upon injection of artificial CSF (control) or AntimiR204.

H   Dot plot showing the density of BrdU$^+$ cells (progeny of NSCs) in the RMS and in the OB 7 days after artificial CSF or AntimiR204 injection.

Data information: See also Fig EV2. All fluorescent images are full *Z*-projections of confocal *Z*-stack, (A' and B') are orthogonal projections through the *Z*-stack. Abbreviations: LRC, label-retaining cell, TAPs, transit amplifying progenitors; SEZ, subependymal zone; LV, lateral ventricle; WT, wild type; qNSC, quiescent neural stem cell; aNSC, activated neural stem cell; RMS, rostral migratory stream, OB, olfactory bulb; CTR, control. Data are shown as mean ± SEM; each symbol represents independent biological replicate; significance was tested by non-parametric Kruskal–Wallis ANOVA; *P value < 0.05, **P value < 0.01, ***P value < 0.001. Scale bars (A, A', B, B') 20 μm, (F, G) 50 μm.

cells 7 days after plating (Fig 5A). As NSCs have limited long-term self-renewal capacity in this culture (Costa *et al*, 2011) in agreement with absence of miR-204, we assessed whether co-culturing with ChP increased the abundance of GFAP$^+$ stem cells. Indeed, the size of cellular clusters containing both neuroblasts and GFAP-positive NSCs showed a significant increase in cluster size due to more GFAP-positive NSCs in the ChP co-culture (Fig 5C–E). Notably, the number of neuroblasts was not affected (Fig EV4D). The effect on NSCs numbers was, however, significantly decreased when the ChP was pre-incubated with GW4869 or AntimiR204 1 day before the co-culture (Figs 5C, F and G, and EV4A–D). The number of GFAP-positive NSCs was reduced to almost 50% of the number of GFAP$^+$ cells in the SEZ/ChP co-culture (Fig 5C). Moreover, the ChP co-culture increased the proportion of Ki67$^+$ GFAP$^+$ cells, suggesting proliferation as a major process underlying increase in cluster size (Fig EV4E and F). Also, this increase in the proliferation of GFAP$^+$ cells mediated by ChP co-culture was reduced by GW4869 inhibitor or miR-204 AntimiR204 treatment (Fig EV4E and F). These data, therefore, identify the ChP as major source of miR-204 regulating the balance between self-renewal and differentiation of NSC *in vitro*.

Choroid plexus-specific inhibition of miR-204 reduces the number of qNSCs

As *in vitro* experiments suggested a notable influence of ChP-released miR-204 on NSC behavior, we performed a ChP-specific inhibition of miR-204 *in vivo* using tough decoys constructs comprising of an imperfect RNA hairpin structure that harbors two opposing miR-204 binding sites (Haraguchi *et al*, 2009). For the

construct delivery, we used adeno-associated viruses (AAVs) serotype 5. We injected AAV5 encoding for scrambled or miR-204-specific tough decoys into the lateral ventricle twice with 3-day interval between the injections (Figs 6A and EV5A). The AAV5 transduced exclusively ChP cells after intraventricular delivery without any transduction of cells in the SEZ as revealed by GFP expression (Figs 6B and C, and EV5B and C). Blocking miR-204 selectively in the ChP resulted in a 22-fold decrease of miR-204 compared to the scrambled control 7 days after transduction (Figs 6D and EV5D). Notably, the down-regulation of miR-204 (Figs 6D and EV5D) induced significant transcriptional changes of 41 genes in the ChP (including seven predicted miR-204 targets, Fig EV5E and F, and Table EV8). We did not observe any change in signaling molecules involved in neurogenesis control such as *Tgfβ*, *Fgf2*, *Vegf-a*, *Lif,* or *Slit* (Sawamoto *et al*, 2006; Calvo *et al*, 2011; Silva-Vargas & Doetsch, 2014; Silva-Vargas *et al*, 2016), suggesting that the interference with miR-204 (Fig EV5D) did not induce general changes in ChP physiology (Fig EV5G) that could thereby indirectly affect the number of qNSCs. Therefore, we addressed the effect of decreased miR-204 levels in the ChP on neurogenic priming. We quantified the number of BrdU$^+$ cells with detectable levels of MEIS2 and MCM6 protein after ChP-specific miR-204 inhibition (Fig 6E–J). Our analysis revealed a significant increase of LRCs with detectable levels of MEIS2 or MCM6 upon down-regulation of miR-204 in the ChP compared to control-treated animals, suggesting that LRCs had entered the cell cycle and were progressing toward neuronal differentiation when miR-204 was depleted (Fig 6E–J). Concomitantly, ChP-specific inhibition of miR-204 significantly reduced the number of cells that were BrdU$^+$, but immunonegative for Ki67 and DCX, a marker profile characteristic for bona-fide LRCs

Figure 4.   Choroid plexus is a main source of the miR-204 that is released into the CSF.

A   Micrographs of *in situ* hybridization for miR-204 in an adult mouse brain section. (A' and A") are magnifications of boxed areas in (A or A'), respectively.

B   Dot plot showing miR-204 levels in ChP and SEZ in the adult mouse brain measured by RT–qPCR.

C   Agarose gel of RT–qPCR product loaded after the saturation phase showing presence of miR-204 and U6 in mouse ChP, SEZ, and CSF.

D, E   Plots depicting the number and size of EVs isolated from human CSF (D) and miR-204 levels (E) in EVs and EV-free CSF (*n* = 2).

F   Agarose gel of RT–qPCR analysis depicting levels of miR-204 in the EV-free supernatant and EV containing fraction of human CSF loaded at the saturation phase.

G   Micrographs of transmission electron microscopy imaged extracellular vesicles (EVs) isolated from sham-treated (upper row) and GW4869-treated animals (lower row). (G' and G") are magnifications of boxed areas in overview images to the left.

H   Dot plot depicting miR-204 levels in the CSF isolated 2 h after the ventricular injection of GW4869 inhibitor.

Data information: Abbreviations: STR, striatum; ChP, choroid plexus; CSF, cerebrospinal fluid; CTX, cortex; LV, lateral ventricle; SEZ, subependymal zone; OB, olfactory bulb; EV, extracellular vesicle; CTR, control; ISH, *in situ* hybridization. Data are shown as mean ± SEM; each single dot represents an independent biological replicate; significance was tested using Kruskal–Wallis ANOVA; *P value < 0.05, ***P value < 0.001. Scale bars (A) 300 μm, (A') 100 μm, (A") 25 μm, (G) 1 μm, (G', G") 200 nm.

(Fig 6K–M). These results demonstrate a key role of ChP-released miR-204 in regulating the balance between the activation and quiescence of qNSCs. Taken together, our data suggest that the deregulation of neurogenic priming of qNSCs in absence of the ChP-released miR-204 instructs pre-mature neurogenic differentiation of qNSCs.
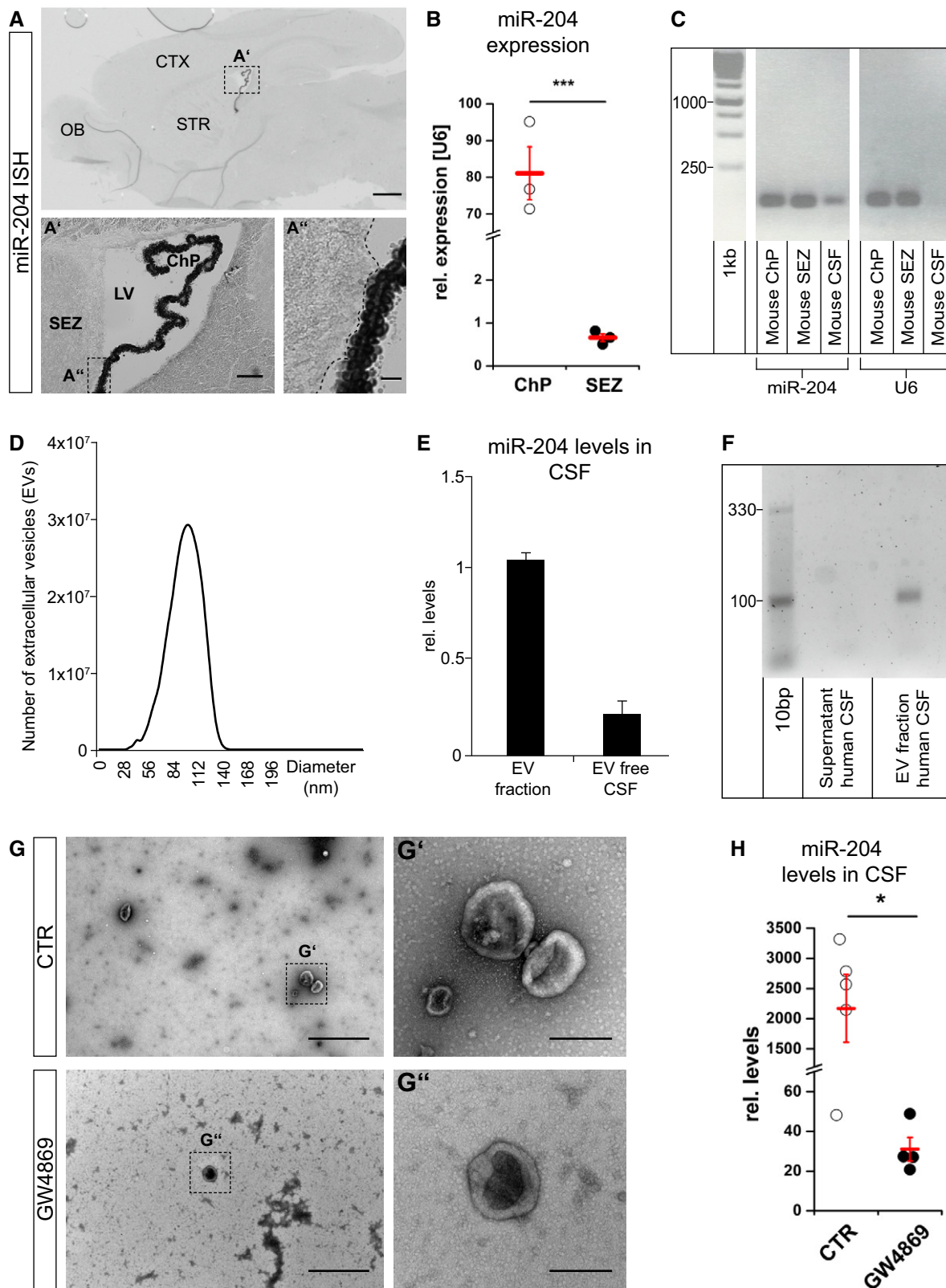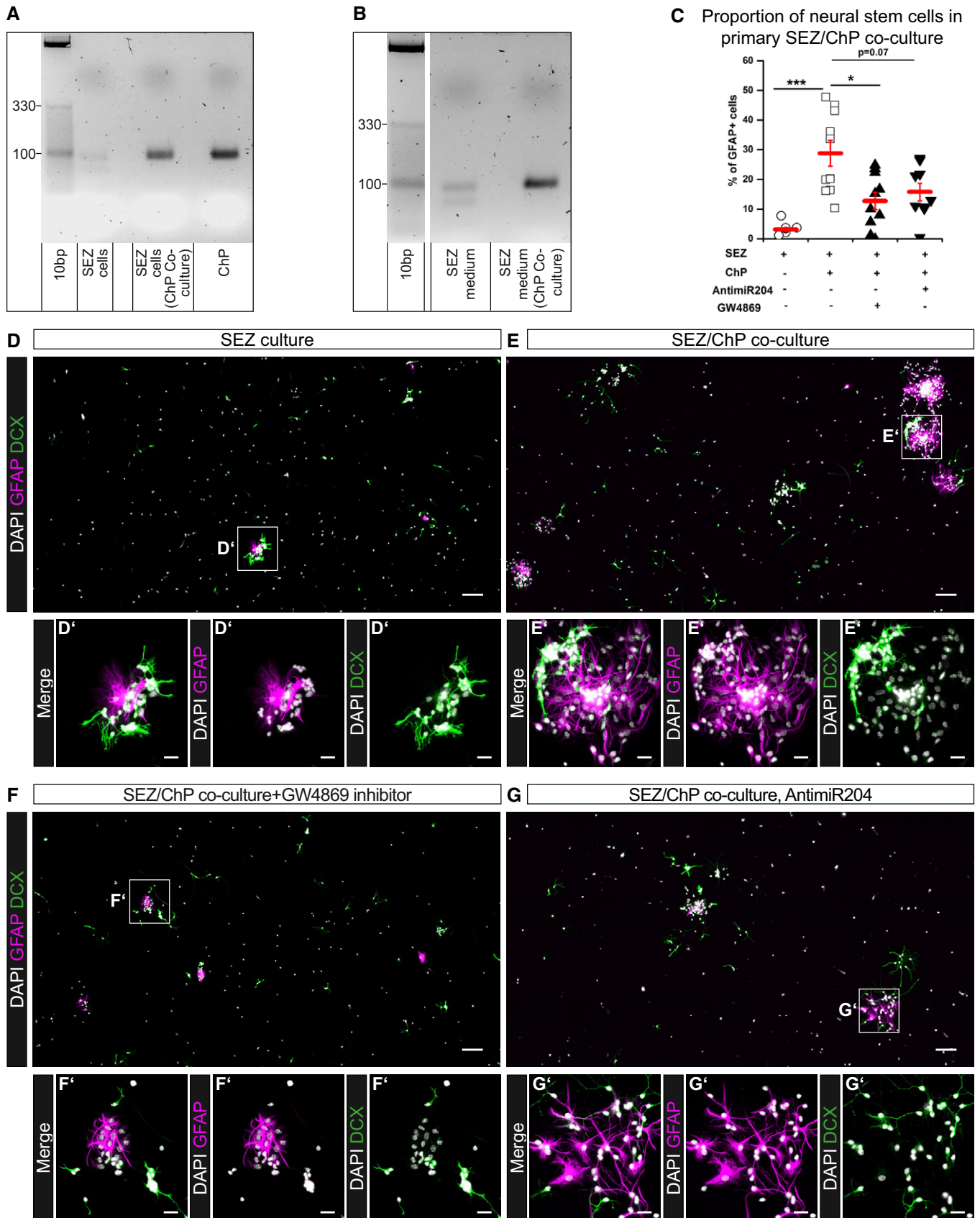

Figure 4.

Figure 5.

Figure 5. NSCs in the SEZ take up ChP-released miR-204.

A Gel pictures of the saturation phase of RT–qPCR analysis for miR-204 in SEZ primary culture cells, ChP co-culture, and ChP explants 7 day post-preparation.
B Gel electrophoresis of RT–qPCR analysis loaded at the saturation phase for miR-204 in SEZ culture medium and SEZ medium from the ChP co-culture.
C Dot plot showing the proportion of neural stem cells (GFAP$^+$) out of DAPI$^+$ cells in primary SEZ/ChP co-culture with or without treatment with GW4869 inhibitor or AntimiR204.
D–G Micrographs depicting the cellular compositions of SEZ cultures after co-culturing with control-treated, GW4869 inhibitor-treated, or AntimiR204-treated ChP 7 days after plating. Boxed areas correspond to the higher magnification images in adjacent panels (D', E', F', G').

Data information: See also Fig EV4. Abbreviations: SEZ, subependymal zone; ChP, Choroid plexus. Data are shown as mean ± SEM; each single dot represents an independent biological replicate; significance was tested using Kruskal–Wallis ANOVA; *P value < 0.05, ***P value < 0.001. Scale bars (D, E, F, G) 100 μm, (D', E', F', G') 20 μm.

Discussion

Here, we revealed a novel mechanism to keep qNSCs in a primed neurogenic state. Namely, ChP releases miR-204 and thereby regulates qNSC numbers in the SEZ of the adult mouse brain. Antagonizing miR-204 *in vivo* either by antagomir injection or by tough decoys delivered specifically to the ChP decreased priming of qNSCs and induced their pre-mature differentiation toward the neuronal lineage, indicated by an increase in the number of neuroblasts. This phenotype is well consistent with the targets of miR-204 that regulate proliferation and neurogenesis. High levels of miR-204 maintain qNSCs by retaining its targets at lower levels and thereby interfering with activation and differentiation, while the increase of these targets upon miR-204 inhibition results in NSC progression in the lineage toward neuroblasts and NSC depletion. Our data, therefore, reveal a novel mechanism of cross-talk from the ChP to the adult NSC niche, mediating neurogenic priming and in turn controlling the number of qNSCs. Thus, miRNA-mediated post-transcriptional control regulates the balance between differentiation and maintenance of primed qNSCs. Our data, therefore, also provide the first mechanistic basis for maintenance of the neurogenic potential of stem cells in the micro-niche close to the ChP embedded in the otherwise largely gliogenic brain environment. Indeed, when these cells are transplanted outside of the neurogenic niche, they differentiate into glial cells (Seidenfaden et al, 2006).

Interestingly, neurogenic priming appears to rely on different mechanisms during development and adulthood. During development, the strong translational repression complex elF4E1/4E-T traps mRNA encoding for neurogenic transcription factors to prevent differentiation (Yang et al, 2014), while we show here

miRNA-mediated mechanisms arising from the ChP as signaling mechanism in the adult brain. The mechanism operating in adulthood may be better suited to allow reaction to environmental stimuli such as inflammation (Baruch et al, 2014; Balusu et al, 2016), brain injury sensed by the ChP (Lun et al, 2015), or aging. This concept is supported by the reduction of miR-204 levels in the CSF after brain injury in the striatum (Liu et al, 2015), which correlates with an increase of neurogenesis in the SEZ (Carlen et al, 2009; Ernst et al, 2014). Similarly, the levels of miR-204 decrease with aging in the ChP, consistent with the reduction in the number of NSCs and neurogenesis with aging (Shook et al, 2012) and the proposed role of the ChP in regulating age-depended changes in neurogenesis (Silva-Vargas et al, 2016). Thus, the ChP not only acts as a signaling hub during brain development (Lehtinen & Walsh, 2011; Johansson et al, 2013), but also appears to be a major regulatory center for adult SEZ neurogenesis, including the regulation of number of qNSC (this study), their activation (Silva-Vargas et al, 2016), and migration of newly born neurons (Sawamoto et al, 2006). Indeed, the block of EV production altered not only the number of NSCs, but also number of neuroblasts *in vitro* (Fig EV4D). The privileged location of the ChP at the blood–brain barrier interface allows ChP to sense, integrate, and respond to both local and systemic stimuli by changing its secretome (Marques & Sousa, 2015), including the exosome containing RNA (Balusu et al, 2016). This allows a response to different physiological and pathological conditions distant from the neurogenic niche itself. Indeed, the SEZ-OB system offers a unique opportunity to address such long range controlling mechanisms as the NSCs and their final progeny are not in direct physical contact. Therefore, such a regulatory relay center might be important to adapt the

Figure 6. ChP-specific inhibition of miR-204 decreases neurogenic priming of adult NSCs and the number of qNSCs in the SEZ.

A Schematic representation of the experimental setup to address the effect of ChP-specific miR-204 inhibition on the number of LRCs and neurogenic priming.
B, C Micrographs depicting specific expression of AAV5 encoded GFP in the ChP 7 days after viral delivery in the lateral ventricle. (B' and C') are magnifications of the SEZ and (B" and C") of the ChP.
D Dot plot depicting expression of miR-204 in ChP 7 days after second ventricular injection of AAV5 encoding for miR-204-specific TuD compared to scrambled control.
E–J Micrographs depicting immunoreactivity for MEIS2 (E, F) and MCM6 (H, I) priming factors in the LRCs (BrdU$^+$ only) 7 days after ChP-specific miR-204 inhibition (F, I) and scrambled control (E, H). White arrows point out the primed LRCs, the arrowheads label the MEIS2$^+$ or MCM6$^+$ + LRCs. (G, J) Dot plots depicting the proportion of LRCs immunoreactive for the priming proteins MEIS2 (G) and MCM6 (J) after ChP-specific miR-204 interference.
K, L Micrographs showing the cellular composition in the SEZ 7 days after injection of AVV5 encoding for scrambled control (K) and miR-204-specific TuD (L). Note the reduction of primed LRCs (BrdU$^+$ only, white arrows in K and L) upon TuD-204 injection.
M Dot plot depicting the number of LRCs (BrdU$^+$ only) in the SEZ 7 days after miR-204 inhibition.

Data information: See also Fig EV5. Abbreviations: WT, wild type; OB, olfactory bulb; CTX, cortex; RMS, rostral migratory stream; SEZ, subependymal zone; dpi, days post-injection; ChP, choroid plexus; LV, lateral ventricle; qNSC, quiescent neural stem cell, LRC, label-retaining cell; TuD, tough decoy. Fluorescent images are full Z-projections of confocal Z-stack, except of K' and L' representing orthogonal projection in the single plane. Data are shown as mean ± SEM; each single dot represents independent biological replicate; significance was tested using Kruskal–Wallis ANOVA; *P value < 0.05. Scale bars (B, C) 100 μm, (B', B", C', C") 50 μm, (E, F, H, I, K, K', L, L') 20 μm.
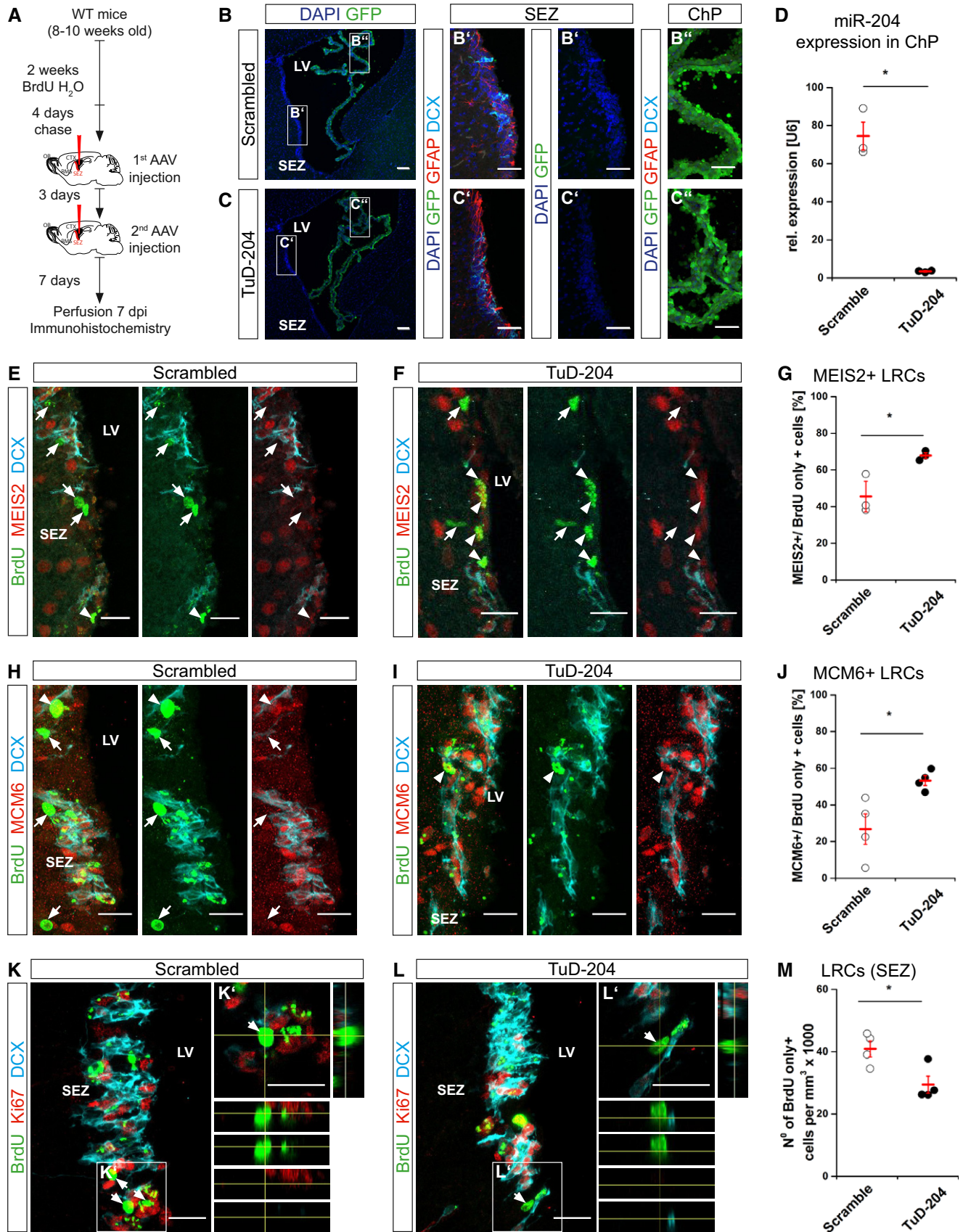
Figure 6.

levels of neurogenesis to environmental signals. It thus serves as a model for controlling stem cell number in other somatic stem cell niches, including hematopoietic or mesenchymal stem cells also characterized by lineage priming (Delorme *et al*, 2009; van Galen *et al*, 2014), long-term self-renewal and plasticity (Nimmo *et al*, 2015).

Materials and Methods

Animal models

All experiments were conducted on 7- to 10-week-old wild-type C57BL/6J or transgenic heterozygous hGFAP-GFP mice (Nolte *et al*, 2001). Animals were kept under standard conditions with access to water and food *ad libitum*. Experimental procedures were approved by our institutional animal care committee and the Government of Upper Bavaria and performed in accordance with German and European Union guidelines under license number 55.2-1-54-2532-150-11.

Primary SEZ culture/ChP co-culture

Primary culture from the subependymal zone (SEZ) was prepared following previously published protocol (Costa *et al*, 2011; Ortega *et al*, 2011). After the purification step, cells were resuspended in neurosphere medium: DMEM/F-12 GlutaMAX™ (Gibco, Thermo Fisher Scientific) supplemented with penicillin–streptomycin (1:100; Gibco, Thermo Fisher Scientific), B27 supplement (1:50; Gibco, Thermo Fisher Scientific), and HEPES buffer solution (1 M; Invitrogen). Cells isolated from a single animal were plated into a single well in a 24-well plate with previously prepared poly-D-lysine(PDL)-coated coverslips (1% in PBS; Sigma) and cultured at 37°C in 5% CO_2 for 1 week. Cell identity was checked by immunocytochemistry for proteins specific for different cell types as previously described (Costa *et al*, 2011; Ortega *et al*, 2011). Stem cells were identified by their astro/radial glial identity by immunocytochemistry for glial fibrillary acidic protein (GFAP). Neuroblasts were identified by expression of doublecortin (DCX).

For co-culturing the SEZ cells with choroid plexus explants, choroid plexuses (ChP) were collected prior to dissection of the SEZ and incubated for 16–24 h at 37°C in neurosphere medium before transferring them into hanging cell culture inserts (Millicell). One choroid plexus explant was placed into each inlet that was after initial culturing (16–24 h) inserted into the well with the primary SEZ cultures. Cultures were fixed after 7 days of co-culturing and analyzed using immunocytochemistry.

Chemical inhibition of EVs production *in vitro* was performed during the incubation period of the ChP in the neurosphere medium by addition of a GW4869 inhibitor, neutral sphingomyelinases inhibitor (nSMAse2) in a final concentration of 10 μM. miR-204 inhibition was achieved by adding 5 μg of Antagomir204 (GE Healthcare) to the neurosphere medium for 16–24 h before transferring the ChP to the SEZ culture. To address the effect of the EVs or miR-204 inhibition, primary culture cells were fixed, stained, and analyzed after 7 days. In addition, primary cells, conditioned medium, and choroid plexus were analyzed 7 days after plating by real-time qPCR.

Assessment of cohort size of LRC

To address the cohort size of LRC within the pool of qNCSs, the hGFAP-GFP animals were given the BrdU water for 2 weeks followed by 2 weeks of chase, SEZ was dissected and dissociated to single cells as previously described (Beckervordersandforth *et al*, 2010; Fischer *et al*, 2011) and plated on poly-D-lysine-coated coverslips. Cells were fixed 2–3 h after plating and immunostained with GFP, CD133, and BrdU antibodies as described in immunocytochemistry paragraph.

To perform *Meis2* RNA FISH, SEZ primary cells were isolated from BrdU-treated WT animals (2 weeks of BrdU water followed by 2 weeks normal drinking water) as described above and fixed 2–3 h after plating.

Human and mouse CSF sample collection

Human CSF samples were obtained from patients (two females, age 39 and age 41) that underwent a lumbar puncture to exclude intracranial hemorrhage or inflammatory diseases of the CNS and who were considered healthy based on normal values for CSF (color, cell count, and total protein). CSF analysis was approved by the institutional review board of Erlangen University Hospital (ethics committee number 3950), and patients gave informed consent. After lumbar puncture, protease inhibitor was added to CSF according to the manufacturer's instructions (Roche) and CSF was directly frozen at −80°C.

Independently, the extracellular vesicles were isolated from human CSF for the miRNA RT–qPCR. CSF was collected from two individuals (male, age 60 years and female, age 59) at Göttingen University Memory Clinic, Department of Psychiatry, Germany. The procedure was approved by the local ethics committee (Institutional review board (IRB) approval 02/05/09, Ethics committee of the University Medical Center). CSF was centrifuged at 2,000 rcf for 10 min at room temperature, aliquoted, and frozen at −80°C within 30 min.

For collecting mouse CSF samples, mice were anesthetized by intraperitoneal injection of Ketamine (Ketaminehydrochloride, 100 mg per kg of body weight) and Rompun (Xylazin, 20 mg/kg body weight), followed by puncturing the cisterna magna with a glass capillary. Only clear CSF samples devoid of blood contamination were further processed and analyzed. CSF samples were frozen on dry ice directly after collection and stored at −80°C.

Extracellular vesicles (EVs) isolation and RNA extraction

To isolate the EVs from the CSF, two independent methods were used. First, the EVs from the mouse and human CSF were isolated with the miRCURY Exosome Isolation Kit—cells, urine, and CSF (Exiqon) according to the manufacturer's instructions. The volumes were scaled down for 10 times, and the centrifugations steps were adjusted to 10,000 rcf. After the last centrifugation step, 1 ml of RLT buffer (Qiagen) was added to the supernatant and 350 μl to the exosomal pellets. RNA was then extracted using the miRNeasy Mini Kit (Qiagen) according to the manufacturer's instructions and retrotranscribed. To address the miRNA-204 expression, real-time qPCR was performed and the product of the final saturation phase was loaded on the 2% agarose gel.

Second, for the miRNA RT–qPCR from human CSF, extracellular vesicles were prepared as previously described (Stuendl *et al*, 2016) by sequential centrifugation of CSF at 4°C. The fluid was centrifuged two times at 4,500 rcf for 10 min, 30 min at 10,000 rcf, and at 100,000 rcf for 60 min, with the supernatant collected each time. The supernatant was subjected to ultracentrifugation at 100,000 rcf to obtain the EV pellet and the EV-free supernatant. EV pellet was thoroughly homogenized in 1 ml TRI reagent and incubated at room temperature for 5 min. 200 μl of chloroform was then added and mixed by vigorous shaking, followed by a 5-min incubation step at RT. The mixture was centrifuged at 12,000 rcf for 15 min until phase separation and the topmost aqueous RNA-containing layer transferred into a new 1.5-ml tube. The RNA was precipitated using 500 μl of isopropanol overnight at −20°C. After centrifugation at 12,000 rcf for 30 min, the supernatant was discarded and the pellet washed two times (12,000 rcf for 5 min each) with 75% ethanol. The RNA pellet was air-dried and resuspended in 10 μl of water. RNA was quantified using Total Eukaryotic Pico 6000 RNA Assay (Agilent) on the 2100 Agilent Bioanalyzer according to the manufacturer's instructions.

Transmission electron microscopy

To visualize EVs by transmission electron microscopy, 20 μl of undiluted mouse CSF was spotted on a parafilm sheet. Formvar/C-coated hexagonal copper grids (EMS G200H-Cu), which were glow discharged for 10 s, were placed on top of the droplet for 1 min with the coated side of the grid down. The grids were washed 5× in droplets of Milli-Q water, stained with 1% (w/v) uranyl acetate for 10 s, and air-dried for 24 h before imaging on the transmission electron microscope (JEM 1400Plus, JEOL) operating at 80 kV.

Fluorescence-activated cell sorting (FACS)

FACS of different populations from the adult mouse brain subependymal zone (SEZ) was performed as previously described (Beckervordersandforth *et al*, 2010; Fischer *et al*, 2011) from hGFAP-GFP transgenic animals. Following cell types were sorted: quiescent adult neural stem cells (qNSC; hGFAP-GFP⁺, CD133⁺, EGFR⁻), activated adult NSC (aNSC; hGFAP-GFP⁺, CD133⁺, EGFR⁺), and neuroblasts (NB; PSA-NCAM⁺, O4⁻). Finally, dissection of diencephalon from hGFAP-GFP mice was used to sort diencephalon astrocytes (DE; hGFAP-GFP⁺).

To analyze the specificity of the AAVs upon their injection into the lateral ventricle, the SEZ cells were dissociated as described in references above, and cells were analyzed using a FACS Aria II (BD) in BD FACS Flow TM medium. Debris and aggregated cells were gated out by forward scatter (FSC-A) and side scatter (SSC-A); *FSC*-A versus *FSC*-W was used to discriminate doublets from single cells. Gating for GFP⁺ cells was done using non-injected WT animals.

RNA extraction and Real-Time qPCR

Tissue or cells for the RNA extraction (cell culture, FACS purified cells, subependymal zone, or choroid plexus) were collected and homogenized in RLT buffer (Qiagen). Total RNA including micro-RNAs was extracted using the miRNeasy Mini Kit (Qiagen) according to the manufacturer's instructions including the step for the

genomic DNA removal. To extract the RNA from the CSF or the medium used to culture the ChP explant with GW4869 inhibitor, the equal volume of RLT buffer (Qiagen) was added and all following steps described in the user manual were performed. In order to extract the RNA from the cell culture medium from the SEZ culture or SEZ/ChP co-cultures, miRCURY Exosome Isolation Kit—cells, urine, and CSF (Exiqon) were used according to the manufacturer's instructions. The volumes were scaled down for 10 times and the centrifugations steps were adjusted to 10,000 rcf. After the last centrifugation step, 350 μl of RLT buffer (Qiagen) was added to the pellet and the RNA was extracted as described above. The Agilent 2100 Bioanalyzer was used to assess RNA quality. For RT–qPCR and RNA-seq library preparation, only high-quality RNA was used.

Total RNA including microRNA was retrotranscribed with the miScript II RT Kit (Qiagen) using the supplied protocol. 1 μl of cDNA was used for each RT–qPCR in a total volume of 10 μl. Real-time qPCR was performed on a QuantStudio™ 6 Flex Real-Time PCR System (Life Technology) using the miScript SYBR Green PCR Kit (Qiagen) and miScript Primer Assays (Qiagen) for microRNAs that include adapter primers generating PCR product about 150 bp. RT–qPCR for Meis2, Sox11, Arx, Dlx1, and Dlx2 was performed using Quanti Fast SYBR Green PCR Kit (Qiagen) and QuantiTect Primer Assays (Qiagen). RNU6B (U6) was used as a reference small RNA. The expression was analyzed in triplicates. The relative expression of the target gene or microRNA was calculated as $E = 2^{-\Delta C_t}$. ΔC_t was calculated as the difference between the threshold cycle number of the target or microRNA and U6. The standardization of miR-204 levels in the CSF is based on the volume—exactly the same volume of CSF was taken for the total RNA and microRNA isolation and all the samples were further processed in the same way. The qPCR was also used to verify the microRNA knock-down in absence of better alternative established in the field.

Preparation of libraries for RNA-sequencing

cDNA was synthesized from 10 ng (ChP tissue) or 300 pg (FACS sorted qNSCs) of total RNA using SMART-Seq v4 Ultra Low Input RNA Kit for Sequencing (Clontech), according to the manufacturer's instructions. Prior to generating the final library for Illumina sequencing, the Covaris AFA system was used to perform the cDNA shearing, resulting in 200- to 500-bp-long cDNA fragments. The quality and concentration of the sheared cDNA were assessed on Agilent 2100 Bioanalyzer before proceeding to library preparation using MicroPlex Library Preparation kit v2 (Diagenode). Final libraries were evaluated and quantified using an Agilent 2100 Bioanalyzer, and the concentration was measured additionally with Quant-iT PicoGreen dsDNA Assay Kit (Thermo Fisher Scientific) before sequencing. The uniquely barcoded libraries were multiplexed onto one lane and 100-bp paired-end deep sequencing was carried out on HiSeq 4000 (Illumina) that generated ~ 30 million reads per sample.

RNA-seq analysis

Kallisto pipeline (Bray *et al*, 2016) was used to quantify expression of transcripts, and the Sleuth pipeline (Pimentel *et al*, 2017) was used for the statistical analysis. The cutoff for the differentially regulated genes was based on the expression fold change (> 2-fold) and

P-value adjusted for the 10% false discovery rate (*q*-value < 0.05). FastQ files are deposited at NCBI Central. KEGG pathway enrichment was done using the DAVID Bioinformatic Resources V6.8 (Huang da *et al*, 2009).

Histology, immunocytochemistry, and immunohistochemistry

For perfusions, Ketamine (ketaminehydrochloride, 100 mg/kg of body weight) and Rompun (Xylazin, 20 mg/kg of body weight) were used to anesthetize mice. After checking for pain reflexes, mice were transcardially perfused with PBS to wash out the remaining blood followed by perfusion with ice-cold, buffered 4% PFA (~ 50 ml per mouse). Brains were dissected and post-fixed for 1 h in 4% PFA at 4°C before washing with PBS. For the cryosectioning, brains were cryoprotected in 30% sucrose in PBS, mounted in the Tissue-Tek (Sakura), frozen on dry ice, and cut at 16–20 μm thickness (sagittal sections). For free-floating vibratome sections, brains were embedded in 3% agarose and cut at 60–80 μm thickness. Cell cultures were washed with PBS for 10 min at RT and fixed for 30 min in 4% PFA.

Tissue or cells were processed for immunostaining with primary and secondary antibodies. The following primary antibodies were used: anti-BrdU (Abcam, rat, 1:200), anti-doublecortin (DCX, Millipore, guinea pig, 1:1,000), anti-GFAP (Sigma, mouse IgG1, 1:500), anti-GFP (Aves, chicken, 1:500), anti-Ki67 (Novocastra, rabbit, 1:500), anti-MCM6 (Abcam, rabbit, 1:200), anti-MEIS2 (provided by D. Schulte, rabbit, 1:1,000), anti-CD133 (eBioscience, rat, 1:200). For immunostaining, cell culture or sections were incubated with the primary antibody in 0.5% Triton X-100 in PBS and 10% normal goat serum (NGS) overnight at 4°C. Specimen was washed three times in PBS at RT and incubated with Alexa-conjugated secondary antibodies (Invitrogen, 1:500) and DAPI (Roche, 1:1,000) for 2 h at RT followed by another three washing steps with PBS at RT. For the MEIS2 staining, the sections were first blocked 30 min in 0.3% Triton X-100 in TBS + 10% NGS, followed by antibody incubation in 0.3% Triton X-100 in TBS. CD133 staining was performed in 0.1% Triton X-100 in PBS + 10% NGS, followed by incubation with a biotinylated secondary antibody and streptavidin-conjugated fluorochrome. For BrdU staining, sections were treated 12 min with 2 M HCl and neutralized 2 × 10 min by borate buffer with pH 8.5. Primary SEZ cells were incubated for 15 min in AR6 buffer (PerkinElmer) in the heat steamer (Oster). Tissue sections and cell cultures were mounted in Aqua-Poly/Mount (Polysciences).

microRNA *in situ* hybridization

For the detection of mature microRNA, digoxigenin-labeled microRNA-specific probes (hsa-miR-204, Exiqon) were used. 16- to 20-μm cryostat sections were first thawed and dried at RT for 1 h. After fixation of the slides with 4% PFA in PBS for 15 min, slides were washed in PBS and treated with proteinase K in PBS for 5 min. Subsequently, slides were washed with 0.2% glycine in TBS, followed by two washing steps in TBS and two incubation steps in methylimidazole solution (0.13 M 1-methylimidazole, 300 mM NaCl). Afterward, 500 μl EDC solution (0.16 M EDC in methylimidazole solution) was prepared and added to each slide and incubated for 1–2 h. Slides were then washed once in 0.2% glycine in TBS and twice in TBS followed by 30 min of acetylation with

triethanolamine, HCl, and acetic anhydride. After another two washing steps in TBS, slides were pre-hybridized with 500 μl hybridization buffer (50% formamide, 5× SSC, 5× Denhardt's solution, 250 μg/ml yeast tRNA, 2% blocking reagent, 0.1% Chaps, 0.5% Tween) for at least 1 h at RT. For hybridization, *in situ* probes were activated by boiling at 85°C for 5 min in hybridization buffer before adding 5 pmol of the probe to the slides. Slides were then covered with glass coverslips and incubated overnight at 20°C below melting temperature of ISH probe. On the next day, slides were washed in SSC, 50% formamide twice for 30 min at hybridization temperature followed by washing steps in SSC and TBS-T. For blocking, 500 μl blocking solution (5% blocking reagent, 10% FCS in TBS-T) was added per slide and incubated for 1 h at RT. Anti-DIG-Fab fragments were diluted 1:1,000 in blocking solution and incubated overnight at 4°C. Afterward, slides were washed twice in TBS and once in detection buffer before adding 400 μl NBT/BCIP solution per slide. The color reaction was developed in the dark at 4°C and stopped in PBS.

Fluorescence *in situ* hybridization in combination with immunostaining

For *Meis2* mRNA detection, digoxigenin-labeled RNA antisense probes were generated by *in vitro* transcription using DIG-labeling mix and T3 polymerase (Roche). *In situ* hybridization was performed on 16- to 20-μm thick cryo-sections from long-term BrdU-treated animals. Sections were post-fixed for 5 min in 4% PFA. After washing steps in PBS and 2× SSC, pre-hybridization was performed with hybridization buffer (50% formamide, 5× Denhardt's solution, 5× SSC, 0.25 mg/ml yeast tRNA, 0.2 mg/ml salmon sperm DNA) for 2.5 h at RT. After addition of the probe (final conc. 1 ng/μl) to the hybridization buffer, the mixture was heated up to 85°C for 5 min and immediately placed on ice for 5 min. The buffer was applied onto the slides and covered with coverslips. Hybridization was carried out in a chamber containing formamide/SSC for 12 h at 65°C. Post-hybridization washes were performed at 65°C for 5 min in 5× SSC, followed by 20 min in 2× SSC and 20 min in 0.2× SSC/50% formamide. Slides were allowed to cool down for 30 min at RT. Subsequently, slides were washed twice in 0.2× SSC for 5 min. Endogenous peroxidase activity was quenched by incubation in 3% H_2O_2 (w/w) for 15 min. Slides were washed once for 5 min in 1× SSC and 3 × 5 min in TBS followed by 30 min blocking in TNB blocking buffer (0.1 M Tris–HCl, 0.15 M NaCl, 0.5% (w/v) TSA blocking reagent, PerkinElmer). Slides were incubated in anti-DIG-POD Fab fragments (1:350; Roche) diluted in TNB buffer for 2 h in a humidified chamber followed by washing steps in TBS. For the TSA amplification, TSA compound was diluted 1:60 in amplification diluent (Opal kit, PerkinElmer), applied onto the sections, and incubated for 10 min at RT in the dark followed by washing steps in TBS. Slides were next incubated for 45 min in pre-warmed AR6 buffer (PerkinElmer) in a heat steamer (Braun), cooled down to RT, washed 3 × 5 min with TBS-T, and processed for immunohistochemistry. The sections were blocked for 30 min in 0.3% Triton X-100 in TBS + 10% NGS, followed by primary antibody incubation overnight at 4°C. Following antibodies were used: anti-MEIS2 (provided by D. Schulte, rabbit, 1:1,000), anti-BrdU (Abcam, rat, 1:50), anti-doublecortin (DCX, Millipore, guinea pig, 1:2,000). On the next day, washing in TBS-T was performed for 3 × 10 min and sections were incubated with Alexa-conjugated secondary antibodies (Invitrogen,

1:750) for 1 h at RT followed by washing steps in TBS. Signal was post-fixed with 4% PFA for 5 min followed by washing steps in TBS. DAPI (Roche, 1:1,000) was added for 10 min. After final washing, slides were embedded with Aquapolymount (Polysciences).

To perform Meis2 RNA FISH at the single-cell level, primary SEZ cells were isolated and fixed 2–3 h after plating as described above. The protocol was the same as described for the sections above with some minor variations. BrdU treatment was done ahead of the FISH protocol in 70% formamide with 2× SSC for 7 min at 95°C on a preheated microscope slide. After FISH signal amplification with TSA-Cy5 (1:70 in TSA amplification buffer, PerkinElmer), sequential immunocytochemistry was performed with mouse anti-Meis2 (Sigma, 1:1,000) in TBS-T and Alexa-conjugated secondary antibody AF594 (Invitrogen, 1:1,000), followed by incubation with anti-doublecortin (DCX, Millipore, guinea pig, 1:1,000) and anti-BrdU (Abcam, rat, 1:250) in TBS-T. Doublecortin was fluorescently labeled with Cy3 (Jackson Immuno Research, 1:1,000) and BrdU with AF488 (Invitrogen, 1:1,000). At the end, nuclei were stained with DAPI and coverslips were mounted with ProLong Diamond (Thermo Fisher Scientific).

Luciferase constructs and reporter assay

Luciferase constructs containing a part of the 3′UTR of the putative target gene with the predicted miR204 target sites were cloned by using the StrataClone PCR cloning kit and subcloned into the pmiRGlo Dual-Luciferase miRNA Target Expression Vector (Promega). Corresponding 3′UTRs with the mutation in putative miRNA binding site (two changed nucleotides) were designed and purchased as GeneArt Strings DNA Fragments (Thermo Fisher Scientific) and cloned directly into the pmiRGlo Dual-Luciferase miRNA Target Expression Vector. All constructs and sequences are available upon request. For the transfection, HEK293T cells were cultured in DMEM (low glucose, GlutaMAX™ Supplement, pyruvate, Gibco, Thermo Fisher Scientific), containing 10% FCS and penicillin–streptomycin (1:100, Gibco, Thermo Fisher Scientific) at 37°C in 5% CO_2. Twenty-four hours prior to transfection, cells were plated in a 24-well plate with the density 8×10^4 cells per well. On the next day, transfection with the pmiRGlo Dual-Luciferase miRNA Target Expression Vector containing 3′UTR of target genes (200 ng) together with pre-miRNA 204 or pre-miRNA negative control (15 pmol, Exiqon) was performed using Lipofectamine® 2000 Reagent (Thermo Fisher Scientific) according to the manufacturer's protocol. Twenty-four hours later, luciferase reporter assays were performed using the Dual-Luciferase Reporter Assay System (Promega) according to the manufacturer's instructions. For measuring luciferase activity, a Berthold Centro XS LB 960 microplate luminometer was used.

BrdU label retaining

Mice were given 5-bromodeoxyuridine (BrdU, 1 mg/ml, Sigma) in drinking water (with 1% sucrose) for 2 weeks followed by 2 weeks normal drinking water for labeling slowly dividing cells.

Stereotactic injections

For stereotactic injections, animals were anaesthetized by intraperitoneal injection of fentanyl (0.05 mg/kg), midazolam (5 mg/kg), and medetomidine (0.5 mg/kg). Anesthesia was antagonized by injection of buprenorphine (0.1 mg/kg), atipamezole (2.5 mg/kg), and flumazenil (0.5 mg/kg). Mice were injected with 2 µl of artificial CSF or Antagomir204 (GE Healthcare; Wang *et al*, 2012)—5 µg diluted in artificial CSF or 3–4 µl of AAV-scramble control or AAV-TuD-204 viruses, serotype 5 (Tebu-bio) into the lateral ventricle (coordinates relative to bregma in mm): −0.5 anterior/posterior, 1.2 medial/lateral, and −2.2 to 1.8 dorsal/ventral from dura. The miR-204-specific antagomirs or aCSF was injected in the LV in the second week of the chase period to the animals that had received BrdU in drinking water before. Animals were sacrificed 1 week after the injection. AAVs were injected into the lateral ventricle twice with a 3-day interval, first after 4 days of chase and second time after 7 days of chase. Choroid plexus for the transcriptome analysis or qPCR and SEZ for the FACS analysis were isolated 1 week after second AAV injection. For the immunostaining, the animals were perfused 7 days after the second injection.

To inhibit the EVs secretion in the ChP *in vivo*, mice were injected with the mixture containing 2 µl GW4869 inhibitor (4.3 mM stock in DMSO) + 3 µl PBS or 2 µl DMSO + 3 µl PBS into the lateral ventricle as described above. After 2 h, CSF was isolated (see "Human and mouse CSF sample collection" paragraph) and directly frozen at −80°C.

Cell death assay

To assess cell death, the ApopTag Red *In Situ* Apoptosis Detection Kit (Millipore) was used according to the manufacturer's instructions.

Target prediction and GO term analysis

MicroRNA-target predictions were performed using different online target predictions tools (http://www.targetscan.org/, http://www.microrna.org/, http://www.exiqon.com/microrna-target-prediction, http://starbase.sysu.edu.cn/). Venn diagram analysis was performed overlapping neural stem cell signatures from three different publications (Beckervordersandforth *et al*, 2010; Codega *et al*, 2014; Llorens-Bobadilla *et al*, 2015). Beckervordersandforth and colleagues defined the stem cell signature genes as the ones having higher expression compared to diencephalon astrocytes but lower as in the progeny of neural stem cells (DE < NSC < progeny). From Codega *et al*, 2014 genes that are lower or equally expressed in qNSCs as in aNSC very taken for the analysis (qNSC ≤ aNSC). Genes identified as neural stem cell-specific transcripts in Llorens-Bobadilla *et al*, 2015 show lower levels in qNSCs compared to neuroblasts (qNSC ≪ NB). Overlay of these three gene sets resulted in 74 common genes presented in the Venn diagram. GO term analysis of these 74 genes and their subset (predicted miR-204 targets) was performed using DAVID Bioinformatics Resources 6.8 (http://david-d.ncifcrf.gov).

Microscopy and quantification

All sections were photographed and analyzed with an Olympus FV1000 laser-scanning confocal microscope using the FW10-ASW 4.0 software (Olympus) or with Leica SP8X upright confocal microscope using Las X software (Leica). Quantitative analysis of the SEZ

in all experiments was done at least on three sections from ≥ 3 independent biological replicates. The SEZ was defined as a band of tissue with densely packed cell somata of DAPI$^+$ and DCX$^+$ cells. Quantifications were performed using ImageJ software to analyze confocal Z-stacks, and cells were rotated in orthogonal planes to verify double labeling or with Imaris V6.3 software (Bitplane) in the 3D view and Fiji was used for labeling. For the RMS and OB quantification, one section from at least three independent animals was taken. In the RMS, the area of 200×600 μm around the elbow (most ventral region of the RMS) was quantified. In the OB, an area with the size 300×700 μm was quantified. In the selected areas of the RMS and the OB, the number of BrdU- and DCX-positive cells was quantified using Imaris V6.3 software (Bitplane). Pictures of the primary SEZ/ChP co-culture were taken at fluorescent Microscope Axio Imager M2 (Zeiss) using ZEN software (Zeiss). The quantifications were performed in the ZEN software (Zeiss) or ImageJ software, counting 20–25 randomly taken pictures per condition. The number of GFAP$^+$, GFAP$^+$ Ki67$^+$, or DCX$^+$ cells is expressed as a percentage out of all counted DAPI$^+$ cells.

Statistical analysis

Numbers of biological replicates can be seen on the dot plots—each single symbol represents an independent biological replicate. All results are presented as a mean ± standard error of mean (SEM). Statistical analysis was performed in Microcal Origin 9.0 using non-parametric Kruskal–Wallis ANOVA to assess for significance. Results were considered significant with $P < 0.05$ (one asterisk). In graphs, two asterisks are used for the values of $P < 0.01$, three asterisks for $P < 0.001$, and four asterisks for $P < 0.0001$.

Data availability

All FastQ files are available at GEO. Accession number: GSE132217.

Expanded View for this article is available online.

Author contributions
MP, TL, and JN conceived the project and experiments. MP, TL, JH, HBH, SZ, EL-B, AS, TM, CV, JE, MM, and CTB performed experiments and analyzed the data. MG, JN, AM-V, DS, REV, MK, SHS, and AF supervised experiments and discussed results. TL, MP, MG, and JN wrote the article with input of DS and AS. We declare that the authors have no competing interests as defined by EMBO Journal, or other interests that might be perceived to influence the results and/or discussion reported in this article.

Conflict of interest
The authors declare that they have no conflict of interest.

References

Agoston Z, Heine P, Brill MS, Grebbin BM, Hau AC, Kallenborn-Gerhardt W, Schramm J, Gotz M, Schulte D (2014) Meis2 is a Pax6 co-factor in neurogenesis and dopaminergic periglomerular fate specification in the adult olfactory bulb. *Development* 141: 28–38

Azim K, Fischer B, Hurtado-Chong A, Draganova K, Cantu C, Zemke M, Sommer L, Butt A, Raineteau O (2014) Persistent Wnt/beta-catenin signaling determines dorsalization of the postnatal subventricular zone and neural stem cell specification into oligodendrocytes and glutamatergic neurons. *Stem Cells* 32: 1301–1312

Balusu S, Brkic M, Libert C, Vandenbroucke RE (2016) The choroid plexus-cerebrospinal fluid interface in Alzheimer's disease: more than just a barrier. *Neural Regen Res* 11: 534–537

Baruch K, Deczkowska A, David E, Castellano JM, Miller O, Kertser A, Berkutzki T, Barnett-Itzhaki Z, Bezalel D, Wyss-Coray T *et al* (2014) Aging. Aging-induced type I interferon response at the choroid plexus negatively affects brain function. *Science* 346: 89–93

Basak O, Krieger TG, Muraro MJ, Wiebrands K, Stange DE, Frias-Aldeguer J, Rivron NC, van de Wetering M, van Es JH, van Oudenaarden A *et al* (2018) Troy+ brain stem cells cycle through quiescence and regulate their number by sensing niche occupancy. *Proc Natl Acad Sci USA* 115: E610–E619

Baser A, Skabkin M, Kleber S, Dang Y, Gülcüler Balta GS, Kalamakis G, Göpferich M, Ibañez DC, Schefzik R, Lopez AS *et al* (2019) Onset of differentiation is post-transcriptionally controlled in adult neural stem cells. *Nature* 566: 100–104

Beckervordersandforth R, Tripathi P, Ninkovic J, Bayam E, Lepier A, Stempfhuber B, Kirchhoff F, Hirrlinger J, Haslinger A, Lie DC *et al* (2010) In vivo fate mapping and expression analysis reveals molecular hallmarks of prospectively isolated adult neural stem cells. *Cell Stem Cell* 7: 744–758

Bonaguidi MA, Wheeler MA, Shapiro JS, Stadel RP, Sun GJ, Ming GL, Song H (2011) In vivo clonal analysis reveals self-renewing and multipotent adult neural stem cell characteristics. *Cell* 145: 1142–1155

Bond AM, Ming G-L, Song H (2015) Adult mammalian neural stem cells and neurogenesis: five decades later. *Cell Stem Cell* 17: 385–395

Bray NL, Pimentel H, Melsted P, Pachter L (2016) Near-optimal probabilistic RNA-seq quantification. *Nat Biotechnol* 34: 525–527

Brill MS, Snapyan M, Wohlfrom H, Ninkovic J, Jawerka M, Mastick GS, Ashery-Padan R, Saghatelyan A, Berninger B, Gotz M (2008) A dlx2- and pax6-dependent transcriptional code for periglomerular neuron specification in the adult olfactory bulb. *J Neurosci* 28: 6439–6452

Calvo CF, Fontaine RH, Soueid J, Tammela T, Makinen T, Alfaro-Cervello C, Bonnaud F, Miguez A, Benhaim L, Xu Y *et al* (2011) Vascular endothelial growth factor receptor 3 directly regulates murine neurogenesis. *Genes Dev* 25: 831–844

Calzolari F, Michel J, Baumgart EV, Theis F, Gotz M, Ninkovic J (2015) Fast clonal expansion and limited neural stem cell self-renewal in the adult subependymal zone. *Nat Neurosci* 18: 490–492

Cameron HA, Glover LR (2015) Adult neurogenesis: beyond learning and memory. *Annu Rev Psychol* 66: 53–81

Carlen M, Meletis K, Goritz C, Darsalia V, Evergren E, Tanigaki K, Amendola M, Barnabe-Heider F, Yeung MSY, Naldini L *et al* (2009) Forebrain ependymal cells are Notch-dependent and generate neuroblasts and astrocytes after stroke. *Nat Neurosci* 12: 259–267

Codega P, Silva-Vargas V, Paul A, Maldonado-Soto AR, Deleo AM, Pastrana E, Doetsch F (2014) Prospective identification and purification of quiescent adult neural stem cells from their *in vivo* niche. *Neuron* 82: 545–559

Colak D, Mori T, Brill MS, Pfeifer A, Falk S, Deng C, Monteiro R, Mummery C, Sommer L, Gotz M (2008) Adult neurogenesis requires Smad4-mediated bone morphogenic protein signaling in stem cells. *J Neurosci* 28: 434–446

Conover JC, Doetsch F, Garcia-Verdugo J-M, Gale NW, Yancopoulos GD, Alvarez-Buylla A (2000) Disruption of Eph/ephrin signaling affects migration and proliferation in the adult subventricular zone. *Nat Neurosci* 3: 1091–1097

Conte I, Carrella S, Avellino R, Karali M, Marco-Ferreres R, Bovolenta P, Banfi S (2010) miR-204 is required for lens and retinal development via Meis2 targeting. *Proc Natl Acad Sci USA* 107: 15491–15496

Costa MR, Ortega F, Brill MS, Beckervordersandforth R, Petrone C, Schroeder T, Götz M, Berninger B (2011) Continuous live imaging of adult neural stem cell division and lineage progression *in vitro*. *Development* 138: 1057–1068

Delorme B, Ringe J, Pontikoglou C, Gaillard J, Langonne A, Sensebe L, Noel D, Jorgensen C, Haupl T, Charbord P (2009) Specific lineage-priming of bone marrow mesenchymal stem cells provides the molecular framework for their plasticity. *Stem Cells* 27: 1142–1151

Deo M, Yu JY, Chung KH, Tippens M, Turner DL (2006) Detection of mammalian microRNA expression by *in situ* hybridization with RNA oligonucleotides. *Dev Dyn* 235: 2538–2548

Donnelly H, Salmeron-Sanchez M, Dalby MJ (2018) Designing stem cell niches for differentiation and self-renewal. *J R Soc Interface* 15: 20180388

Dulken BW, Leeman DS, Boutet SC, Hebestreit K, Brunet A (2017) Single-cell transcriptomic analysis defines heterogeneity and transcriptional dynamics in the adult neural stem cell lineage. *Cell Rep* 18: 777–790

Englund U, Fricker-Gates RA, Lundberg C, Bjorklund A, Wictorin K (2002) Transplantation of human neural progenitor cells into the neonatal rat brain: extensive migration and differentiation with long-distance axonal projections. *Exp Neurol* 173: 1–21

Ernst A, Alkass K, Bernard S, Salehpour M, Perl S, Tisdale J, Possnert G, Druid H, Frisen J (2014) Neurogenesis in the striatum of the adult human brain. *Cell* 156: 1072–1083

Falk S, Bugeon S, Ninkovic J, Pilz GA, Postiglione MP, Cremer H, Knoblich JA, Gotz M (2017) Time-specific effects of spindle positioning on embryonic progenitor pool composition and adult neural stem cell seeding. *Neuron* 93: 777–791 e3

Fischer J, Beckervordersandforth R, Tripathi P, Steiner-Mezzadri A, Ninkovic J, Gotz M (2011) Prospective isolation of adult neural stem cells from the mouse subependymal zone. *Nat Protoc* 6: 1981–1989

Flax JD, Aurora S, Yang C, Simonin C, Wills AM, Billinghurst LL, Jendoubi M, Sidman RL, Wolfe JH, Kim SU *et al* (1998) Engraftable human neural stem cells respond to developmental cues, replace neurons, and express foreign genes. *Nat Biotechnol* 16: 1033–1039

Fricker RA, Carpenter MK, Winkler C, Greco C, Gates MA, Bjorklund A (1999) Site-specific migration and neuronal differentiation of human neural progenitor cells after transplantation in the adult rat brain. *J Neurosci* 19: 5990–6005

Fuentealba LC, Rompani SB, Parraguez JI, Obernier K, Romero R, Cepko CL, Alvarez-Buylla A (2015) Embryonic origin of postnatal neural stem cells. *Cell* 161: 1644–1655

Furutachi S, Miya H, Watanabe T, Kawai H, Yamasaki N, Harada Y, Imayoshi I, Nelson M, Nakayama KI, Hirabayashi Y *et al* (2015) Slowly dividing neural progenitors are an embryonic origin of adult neural stem cells. *Nat Neurosci* 18: 657–665

van Galen P, Kreso A, Wienholds E, Laurenti E, Eppert K, Lechman ER, Mbong N, Hermans K, Dobson S, April C *et al* (2014) Reduced lymphoid lineage priming promotes human hematopoietic stem cell expansion. *Cell Stem Cell* 14: 94–106

Garcion E, Faissner A, ffrench-Constant C (2001) Knockout mice reveal a contribution of the extracellular matrix molecule tenascin-C to neural precursor proliferation and migration. *Development* 128: 2485–2496

Girard F, Eichenberger S, Celio MR (2014) Thrombospondin 4 deficiency in mouse impairs neuronal migration in the early postnatal and adult brain. *Mol Cell Neurosci* 61: 176–186

Haraguchi T, Ozaki Y, Iba H (2009) Vectors expressing efficient RNA decoys achieve the long-term suppression of specific microRNA activity in mammalian cells. *Nucleic Acids Res* 37: e43

Hau AC, Grebbin BM, Agoston Z, Anders-Maurer M, Muller T, Gross A, Kolb J, Langer JD, Doring C, Schulte D (2017) MEIS homeodomain proteins facilitate PARP1/ARTD1-mediated eviction of histone H1. *J Cell Biol* 216: 2715–2729

Huang da W, Sherman BT, Lempicki RA (2009) Systematic and integrative analysis of large gene lists using DAVID bioinformatics resources. *Nat Protoc* 4: 44–57

Ihrie RA, Shah JK, Harwell CC, Levine JH, Guinto CD, Lezameta M, Kriegstein AR, Alvarez-Buylla A (2011) Persistent sonic hedgehog signaling in adult brain determines neural stem cell positional identity. *Neuron* 71: 250–262

Johansson PA, Irmler M, Acampora D, Beckers J, Simeone A, Gotz M (2013) The transcription factor Otx2 regulates choroid plexus development and function. *Development* 140: 1055–1066

Lehtinen MK, Walsh CA (2011) Neurogenesis at the brain-cerebrospinal fluid interface. *Annu Rev Cell Dev Biol* 27: 653–679

Lim D, Tramontin A, Trevejo J, Herrera D, Garcia-Verdugo J, Alvarez-Buylla A (2000) Noggin antagonizes BMP signaling to create a niche for adult neurogenesis. *Neuron* 28: 713–726

Lim DA, Huang YC, Swigut T, Mirick AL, Garcia-Verdugo JM, Wysocka J, Ernst P, Alvarez-Buylla A (2009) Chromatin remodelling factor Mll1 is essential for neurogenesis from postnatal neural stem cells. *Nature* 458: 529–533

Liu C, Zhao L, Han S, Li J, Li D (2015) Identification and functional analysis of microRNAs in mice following focal cerebral ischemia injury. *Int J Mol Sci* 16: 24302–24318

Llorens-Bobadilla E, Zhao S, Baser A, Saiz-Castro G, Zwadlo K, Martin-Villalba A (2015) Single-cell transcriptomics reveals a population of dormant neural stem cells that become activated upon brain injury. *Cell Stem Cell* 17: 329–340

Lun MP, Monuki ES, Lehtinen MK (2015) Development and functions of the choroid plexus-cerebrospinal fluid system. *Nat Rev Neurosci* 16: 445–457

Luo Y, Coskun V, Liang A, Yu J, Cheng L, Ge W, Shi Z, Zhang K, Li C, Cui Y *et al* (2015) Single-cell transcriptome analyses reveal signals to activate dormant neural stem cells. *Cell* 161: 1175–1186

Marques F, Sousa JC (2015) The choroid plexus is modulated by various peripheral stimuli: implications to diseases of the central nervous system. *Front Cell Neurosci* 9: 136

Ming GL, Song H (2012) Adult neurogenesis in the mammalian brain: significant answers and significant questions. *Neuron* 70: 687−702

Mu L, Berti L, Masserdotti G, Covic M, Michaelidis TM, Doberauer K, Merz K, Rehfeld F, Haslinger A, Wegner M *et al* (2012) SoxC transcription factors are required for neuronal differentiation in adult hippocampal neurogenesis. *J Neurosci* 32: 3067−3080

Nimmo RA, May GE, Enver T (2015) Primed and ready: understanding lineage commitment through single cell analysis. *Trends Cell Biol* 25: 459−467

Ninkovic J, Gotz M (2013) Fate specification in the adult brain–lessons for eliciting neurogenesis from glial cells. *BioEssays* 35: 242−252

Ninkovic J, Steiner-Mezzadri A, Jawerka M, Akinci U, Masserdotti G, Petricca S, Fischer J, von Holst A, Beckers J, Lie CD *et al* (2013) The BAF complex interacts with Pax6 in adult neural progenitors to establish a neurogenic cross-regulatory transcriptional network. *Cell Stem Cell* 13: 403−418

Nolte C, Matyash M, Pivneva T, Schipke CG, Ohlemeyer C, Hanisch UK, Kirchhoff F, Kettenmann H (2001) GFAP promoter-controlled EGFP-expressing transgenic mice: a tool to visualize astrocytes and astrogliosis in living brain tissue. *Glia* 33: 72−86

Nomura T, Goritz C, Catchpole T, Henkemeyer M, Frisen J (2010) EphB signaling controls lineage plasticity of adult neural stem cell niche cells. *Cell Stem Cell* 7: 730−743

Noseda M, Karsan A (2006) Notch and minichromosome maintenance (MCM) proteins: integration of two ancestral pathways in cell cycle control. *Cell Cycle* 5: 2704−2709

Ortega F, Costa MR, Simon-Ebert T, Schroeder T, Gotz M, Berninger B (2011) Using an adherent cell culture of the mouse subependymal zone to study the behavior of adult neural stem cells on a single-cell level. *Nat Protoc* 6: 1847−1859

Petrik D, Myoga MH, Grade S, Gerkau NJ, Pusch M, Rose CR, Grothe B, Gotz M (2018) Epithelial sodium channel regulates adult neural stem cell proliferation in a flow-dependent manner. *Cell Stem Cell* 22: 865−878 e8

Pimentel H, Bray NL, Puente S, Melsted P, Pachter L (2017) Differential analysis of RNA-seq incorporating quantification uncertainty. *Nat Methods* 14: 687−690

Ramirez-Castillejo C, Sanchez-Sanchez F, Andreu-Agullo C, Ferron SR, Aroca-Aguilar JD, Sanchez P, Mira H, Escribano J, Farinas I (2006) Pigment epithelium-derived factor is a niche signal for neural stem cell renewal. *Nat Neurosci* 9: 331−339

Ramos AD, Diaz A, Nellore A, Delgado RN, Park K-Y, Gonzales-Roybal G, Oldham MC, Song JS, Lim DA (2013) Integration of genome-wide approaches identifies lncRNAs of adult neural stem cells and their progeny *in vivo*. *Cell Stem Cell* 12: 616−628

Ramos AD, Andersen RE, Liu SJ, Nowakowski TJ, Hong SJ, Gertz C, Salinas RD, Zarabi H, Kriegstein AR, Lim DA (2015) The long noncoding RNA Pnky regulates neuronal differentiation of embryonic and postnatal neural stem cells. *Cell Stem Cell* 16: 439−447

Sawamoto K, Wichterle H, Gonzalez-Perez O, Cholfin JA, Yamada M, Spassky N, Murcia NS, Garcia-Verdugo JM, Marin O, Rubenstein JLR *et al* (2006) New neurons follow the flow of cerebrospinal fluid in the adult brain. *Science* 311: 629−632

Seidenfaden R, Desoeuvre A, Bosio A, Virard I, Cremer H (2006) Glial conversion of SVZ-derived committed neuronal precursors after ectopic grafting into the adult brain. *Mol Cell Neurosci* 32: 187−198

Shaham O, Gueta K, Mor E, Oren-Giladi P, Grinberg D, Xie Q, Cvekl A, Shomron N, Davis N, Keydar-Prizant M *et al* (2013) Pax6 regulates gene expression in the vertebrate lens through miR-204. *PLoS Genet* 9: e1003357

Shook BA, Manz DH, Peters JJ, Kang S, Conover JC (2012) Spatiotemporal changes to the subventricular zone stem cell pool through aging. *J Neurosci* 32: 6947−6956

Silva-Vargas V, Doetsch F (2014) A new twist for neurotrophins: endothelial-derived NT-3 mediates adult neural stem cell quiescence. *Neuron* 83: 507−509

Silva-Vargas V, Maldonado-Soto AR, Mizrak D, Codega P, Doetsch F (2016) Age-dependent niche signals from the choroid plexus regulate adult neural stem cells. *Cell Stem Cell* 19: 643−652

Stuendl A, Kunadt M, Kruse N, Bartels C, Moebius W, Danzer KM, Mollenhauer B, Schneider A (2016) Induction of alpha-synuclein aggregate formation by CSF exosomes from patients with Parkinson's disease and dementia with Lewy bodies. *Brain* 139: 481−494

Trajkovic K, Hsu C, Chiantia S, Rajendran L, Wenzel D, Wieland F, Schwille P, Brugger B, Simons M (2008) Ceramide triggers budding of exosome vesicles into multivesicular endosomes. *Science* 319: 1244−1247

Wang H, Chiu M, Xie Z, Chiu M, Liu Z, Chen P, Liu S, Byrd JC, Muthusamy N, Garzon R *et al* (2012) Synthetic microRNA cassette dosing: pharmacokinetics, tissue distribution and bioactivity. *Mol Pharm* 9: 1638−1644

Wang WX, Fardo DW, Jicha GA, Nelson PT (2017) A customized quantitative PCR microRNA panel provides a technically robust context for studying neurodegenerative disease biomarkers and indicates a high correlation between cerebrospinal fluid and choroid plexus microrna expression. *Mol Neurobiol* 54: 8191−8202

Weinandy F, Ninkovic J, Gotz M (2011) Restrictions in time and space–new insights into generation of specific neuronal subtypes in the adult mammalian brain. *Eur J Neurosci* 33: 1045−1054

Winkler C, Fricker RA, Gates MA, Olsson M, Hammang JP, Carpenter MK, Bjorklund A (1998) Incorporation and glial differentiation of mouse EGF-responsive neural progenitor cells after transplantation into the embryonic rat brain. *Mol Cell Neurosci* 11: 99−116

Yang G, Smibert CA, Kaplan DR, Miller FD (2014) An eIF4E1/4E-T complex determines the genesis of neurons from precursors by translationally repressing a proneurogenic transcription program. *Neuron* 84: 723−739

Zywitza V, Misios A, Bunatyan L, Willnow TE, Rajewsky N (2018) Single-cell transcriptomics characterizes cell types in the subventricular zone and uncovers molecular defects impairing adult neurogenesis. *Cell Rep* 25: 2457−2469.e8